European Journal of Radiology Open 10 (2023) 100467

Contents lists available at ScienceDirect

European Journal of Radiology Open

journal homepage: www.elsevier.com/locate/ejro

Review

Imaging techniques in veterinary medicine. Part II: Computed tomography, magnetic resonance imaging, nuclear medicine

Adelaide Greco [a], Leonardo Meomartino [a,*], Giacomo Gnudi [b], Arturo Brunetti [c], Mauro Di Giancamillo [d]

[a] Centro Interdipartimentale di Radiologia Veterinaria, Università degli Studi di Napoli "Federico II", Via F. Delpino, 1, 80137 Napoli, Italy
[b] Dipartimento di Scienze Mediche Veterinarie, Università di Parma, Via del Taglio, 10, 43126 Parma, Italy
[c] Dipartimento di Scienze Biomediche Avanzate, Università degli Studi di Napoli "Federico II", Via Pansini, 5, 80131 Napoli, Italy
[d] Dipartimento di Medicina Veterinaria, Università degli Studi di Milano, Via Festa del Perdono, 7, 20122 Milano, Italy

ARTICLE INFO

Keywords:
Veterinary radiology
CT
MRI
Nuclear Medicine
Small animals
Horses
Exotic pets
Wild animals

ABSTRACT

Radiography and ultrasonography are the most used techniques in veterinary clinical practice, due to organizational, managerial and, mostly, economic reasons. However, in the last decades, Computed tomography (CT), Magnetic Resonance Imaging (MRI) and, to a lesser extent, Nuclear Medicine (MN) are increasingly used. As we said in the previous article, all the Diagnostic Imaging techniques are actually "indispensable" in Veterinary Medicine, where many patients do not show any symptoms.This second part describes Computed Tomography (CT), Magnetic Resonance (MRI) and Nuclear Medicine techniques in Veterinary Medicine are described.

1. Computed tomography

Computed tomography (CT) has been one of the most important discoveries in diagnostic imaging. As well known, the first clinical CT scan in a human being was obtained on 1st October 1971 in England, using a prototype EMI head scanner. Veterinary surgeons had to wait for ten years before CT scan became available for clinical purposes [1,2].

The evolution of the CT in Veterinary Medicine had the same development as the human one. Although initially, in small animals, the studies mainly focused on the central nervous system (CNS) diseases, today the clinical indications are the same to those for humans. The introduction of multi detector CT (MDCT) technology has deeply transformed the Veterinary Diagnostic Imaging and, nowadays, it is routinely used in small animals, in exotic pets and in horses. The reduced scan time, a key aspect in Veterinary Radiology, and the increased Z-axis resolution allowed studies unimaginable until some decades ago, such as real-time angiography, whole-body scan in oncological patients, 3D rendering techniques, including virtual endoscopy [3].

In Veterinary Radiology, CT scans are "time-consuming" and require a good staff, including radiologists, technicians and anesthetists.

Although, CT is considered a proven and widely used technique in Veterinary Medicine, obtaining good-quality images is not always easy. Computed tomographic gray scale depends on the linear attenuation coefficient and represents how much each tissue absorbs or scatters a given X-ray beam and, in other words, the relative density of the tissues crossed by the X-ray beam. In the veterinary field, it is challenging to set the linear attenuation coefficient of each patients because of the great variability of the patient size, ranging from very small animals (e.g. hamster) to horses.

Another great problem is represented by the patient movements that cause the streak artifacts and, consequently, a reduction of the image quality [4]. For this reason, to avoid any movement and maintain the same position, CT scans on animals require a pharmacological restraint. Anesthesia guarantees good-quality images but deep sedation is also useful in some animals, like traumatized patients or the horses, where CT scans can be performed in a standing positioning.

Control of mechanical ventilation during general anaesthesia is preferred, especially in dogs and cats, though an automatic breathing device, because apnea is mandatory for obtaining good-quality CT images.

Otherwise, the remaining artifacts observed on Veterinary CT images are the same described in humans [4].

* Corresponding author.
E-mail address: leonardo.meomartino@unina.it (L. Meomartino).

https://doi.org/10.1016/j.ejro.2022.100467
Received 21 October 2022; Accepted 7 December 2022

Fig. 1. – Dog undergoing to CT of the abdomen positioned in sternal-abdominal recumbency.

Another essential difference between CT in animals and human beings is the positioning used during the scan. Sternal-abdominal recumbency with the forelimbs and hindlimbs pulled forward and backward, respectively (Fig. 1) is usually adopted for studying the thorax and the abdomen. The same recumbency is used for the skull, but the forelimbs are pulled caudally along the thorax (Fig. 2). Especially in tumors staging, the sternal-abdominal positioning minimizes the occurrence of ground-glass opacities due to the atelectasis in the depending lung portions, while it is more pronounced when dorsal recumbency is used [5]. However, in a study on anesthetized Beagles, the lateral recumbency did not preclude lung CT examination because changes due to the positioning were minimal [6]. In neonatal foals submitted to CT of the thorax, manual alveolar recruitment maneuvers did not eliminate atelectasis but reduced attenuation in non-dependent portions of the lungs [7]. The dorsal recumbency is routenely adopted to study of the vertebral column to avoid the movement artifacts to that anatomical tract (Fig. 3). Sometime, the patient can be positioned in lateral (left or right) recumbency, especially in traumatized animals. Other particular positioning has been proposed for the study of the vertebral column (positional or dynamic CT), the elbow joints (Fig. 4) and the hip joints [8–10].

The so-called "VetMouse Trap™" can be used as an alternative to anesthesia. Even if this device was thought for very small animals, as laboratory animals (mice, rats, etc.), it could be customized to accommodate cats [9]. However, in our opinion, the use this device is recommended only in reptiles or in very quiet patients which do not require the administration of contrast medium. Computed tomography of avians, as well as of reptiles, usually requires general anesthesia while in chelonians anesthesia is necessary only for the studying the head, neck and legs (Figs. 5 and 6) [11].

Due to the hefty weight, CT in horses is challenging since the couch is a critical item of the procedure. This problem can be resolved using special CT devices in which the couch is able to support the horses in different recumbency, in order to include the skull and the neck or the limbs within the gantry [12] or using a special custom-built horse table,

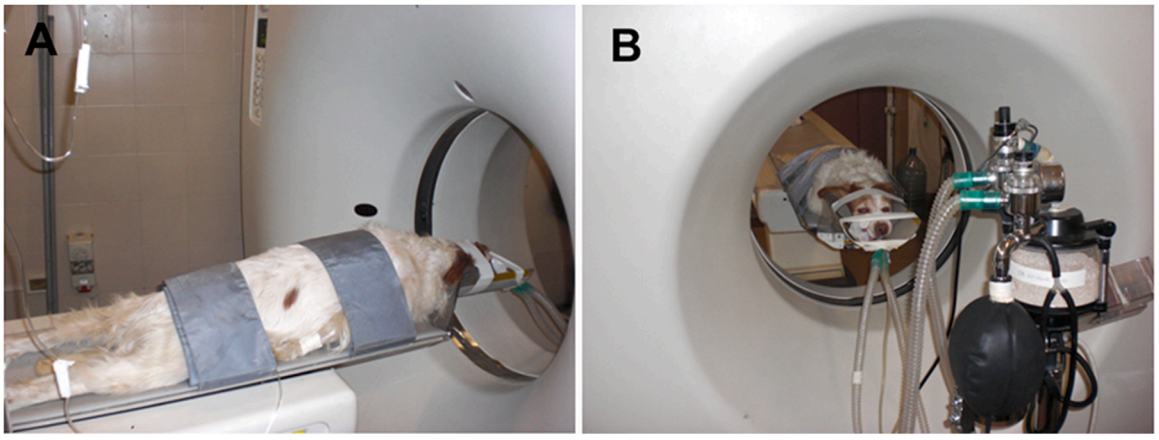

Fig. 2. – Lateral (A) and frontal (B) photos of a dog undergoing to skull CT positioned in sternal-abdominal recumbency with caudally extended forelimbs.

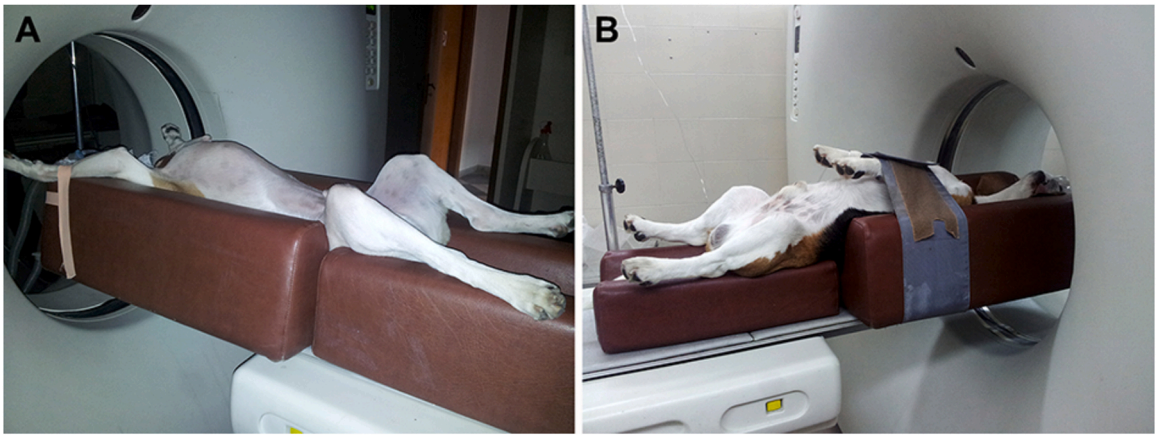

Fig. 3. – Dorsal recumbency for dogs undergoing to CT of the vertebral column. A) Positioning for the thoraco-lumbar tract: the forelimbs are cranially extended. B) Positioning for the cervical tract: the forelimbs are caudally extended.

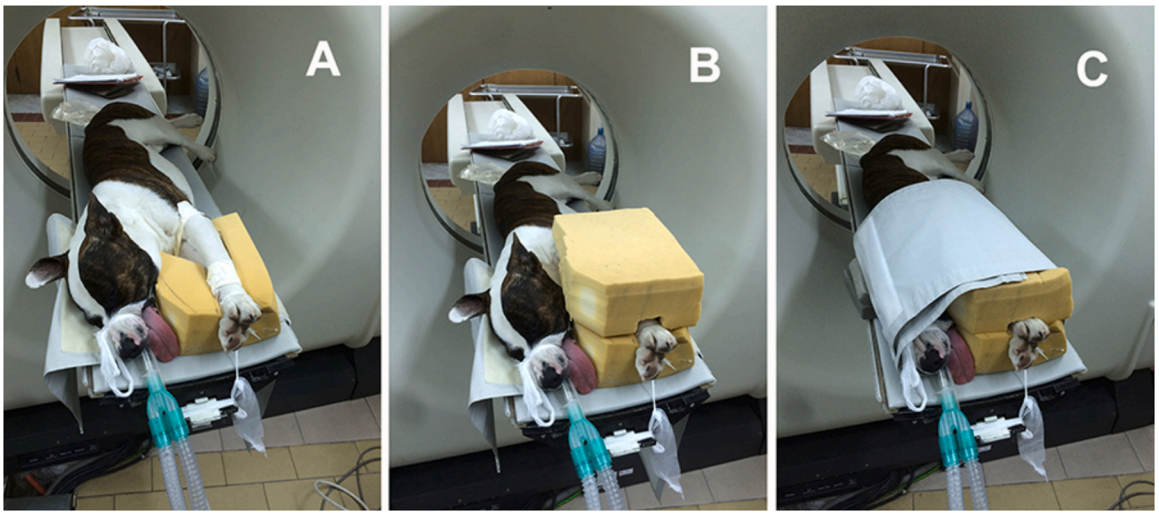

Fig. 4. – Special positioning for elbow CT: the dog is in lateral recumbency with both the forelimbs pulled cranially and lodged in a soft device made by polyurethane (A and B) that removes the air between the skull, the neck and the limbs, for avoiding beam harderning artfacts. Lastly, skull, neck and forelimbs are wrapped together (C), for avoiding streaks artifacts due to respiratory movement.

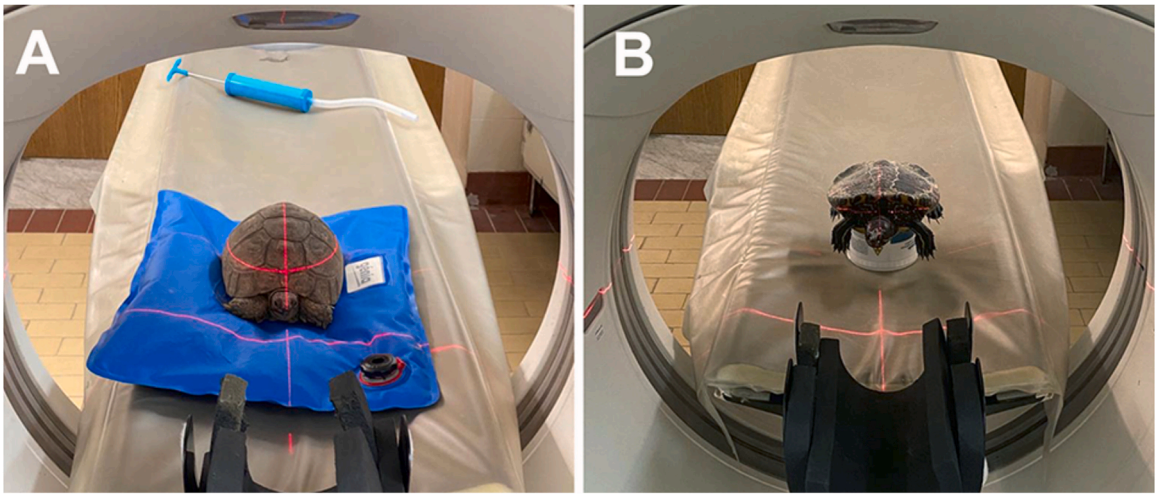

Fig. 5. – Computed tomography on awake tortoises. A) Greek tortoise (*Testudo greca*) undergoing to whole-body CT: in case of very quiet subject, like usually one of this species is, no special restraints are needed. B) Red-eared-slider tortoise (*Trachemys scripta elegans*) undergoing to whole-body CT: the subjects of this species, usually quite lively, are positioned on a jar, or another kind of support, to avoid their limbs touching the couch's surface.

able to support a weight up to six hundred kilograms, linked to the standard CT couch drive. At the Veterinary Hospital of the Department of Veterinary Medicine and Animal Sciences of the University of …, a CT air-cushion technology table it is available for scanning horse in general anesthesia or sedated. The table is placed on the ground and connected to the couch by a neodymium magnet. After the horse has been positioned, using a compressor that maintains a film of air between the table and the floor, the table is lifted a few millimeters. This way a push of 1 kg can move up to 1 ton. This special device allows CT of the head and the cranial neck on sedated horses (Figs. 7 and 8).

In Veterinary Radiology, the current terminology used to define CT image anatomical planes is quite different compared to that of human beings: transversal instead of axial, dorsal instead of coronal, for axial skeleton, the thorax and the abdomen, and frontal, instead of coronal, for the appendicular skeleton; sagittal is used as for human beings [13].

Generally, the slice thickness and the dose index are set according to the size of the patient and the suspected diagnosis, avoiding unnecessary X-ray over-exposure. Usually, the adopted pitch is equal to one. When high-definition or post-processing procedures are required (i.e. 3D reconstruction or virtual endoscopy) sub-millimetric slices with a pitch lesser than one are used.

Contrast media used in Veterinary CT are the same used for human beings. In small animals, a non-ionic iodinated contrast media are usually administered at 400–600 mgI/kg of body weight. Nevertheless, in the literature, higher dosages are reported [14]. The contrast medium is usually injected into cephalic or saphenous veins (jugular veins in very small animals) though manual or automated injection at 1–3 ml/sec administration rate, depending on the volume. When a contrast medium is administered, a second or further post-contrast CT scans are obtained. Scan delay depends on the clinical suspect, the cardiac output and the hearth rate. It can range from a few seconds, in case of arterial vascularization of the lesions, to 1–3 min in other cases [14]. Contrast media can also be administered through different paths (CT dacryocystography, CT myelography, CT gastro-enterography, CT cystography, CT sialography, CT vaginography, CT lymphangiography, CT arthrography) [14].

Severe reactions to the contrast media seem rare in animals and are usually linked to the ionic iodinate contrast agents [14,15].

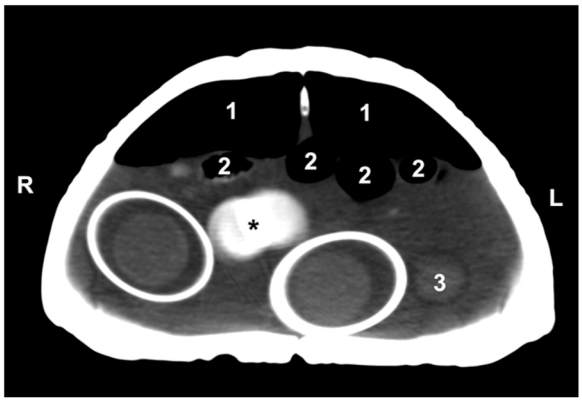

Fig. 6. – Computed tomography image of the middle body of a Greek tortoise (*Testudo greca*) with egg retention. Two eggs with a thick shell and clearly visible yolk are present within the coelomic cavity. Another egg shell is partially visible (asterisk). Legend: 1 = lungs; 2 = meteoric intestinal loops; 3 = fluid filled intestinal loop.

Hypersensitivity to iodinated contrast agents should occur without evidence of prior exposure [16]. In horses, contrast medium is limited in the study of the distal limbs through local intra-arterial administration at the dose of 150–200 mgI/Kg of body weight, with an administration rate of 2 ml/sec [14].

Less frequently, CT is used in ruminants and swines but positioning and protocols are similar to those applied in small animals and horses [17,18].

In small animals, except for the CNS, CT usually represents a second level modality for studying the skeleton, particularly the axial one (skull and spine), the thorax and the abdomen [3]. The use of CT is also described for equine [19], cattle [20], goat [21], sheep [22], swine [23], avian and chelonian [11], reptiles [24], rabbit and rodents [25]. As in human medicine, CT can be used as bone densitometer [26]. In sheep and swine, CT has also been used to evaluate the carcasses' fat content and meat quality of the [27,28].

1.1. Skull

Although widely replaced by MRI, CT is still used as a first-level technique for the diagnosis of the brain's neoplastic, developmental, inflammatory, degenerative or vascular diseases of the brain [3] and for planning the radiotherapy of intracranial tumours [29].

Meningiomas are the most common neoplasia in dogs and cats, and a breed predisposition has been suspected in Golden retrievers, Boxer and miniature Schnauzer (Fig. 9) [30,31]. Astrocytoma and

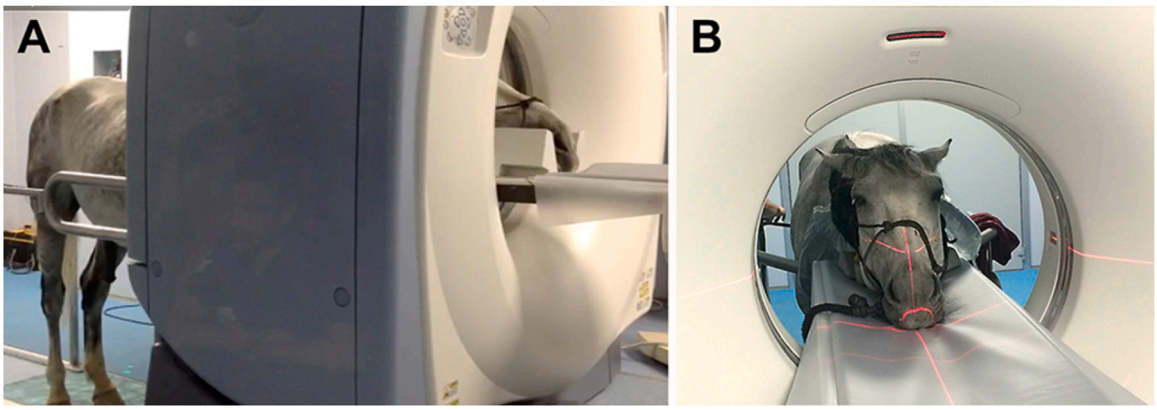

Fig. 7. - Lateral (A) and frontal (B) aspects of a sedated horse undergoing to skull CT in standing position.

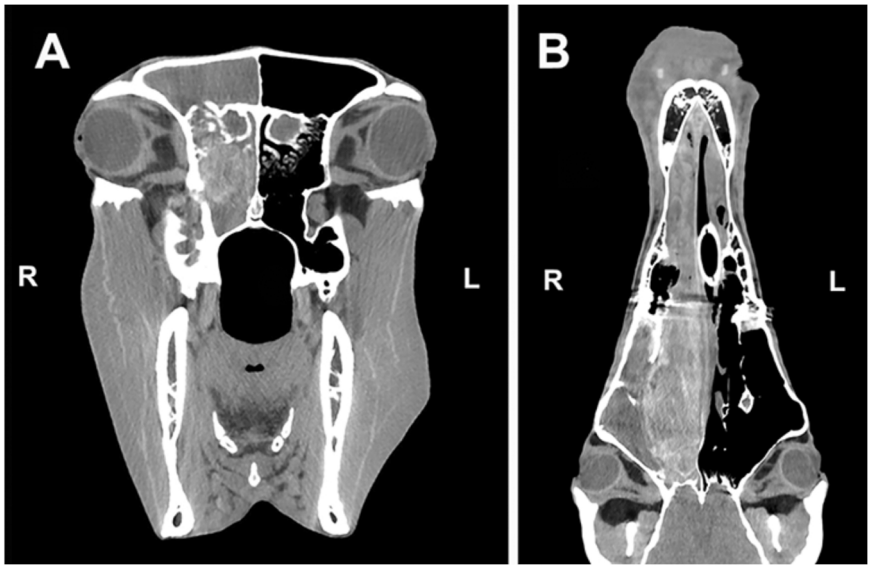

Fig. 8. – Etmoidal hematoma in an adult Italian trotter horse. A) Transverse scan and B) dorsal MPR of the skull. Relatively hyperdense and inhomogeneous blood clots fill the right nasal cavities and the ipsilateral frontal sinus.

Fig. 9. – Meningioma in a 14-years old neutered female Domestic Short Haired cat. A) precontrast and B) postcontrast transverse scan of the skull at the level of the temporomandibular joints. In the pre-contrast scan, the region of left parietal-temporal cortex is slightly hyperdense and, after the contrast administration, markedly enhanced (arrow heads). A "mass effect" is visible to the brain.

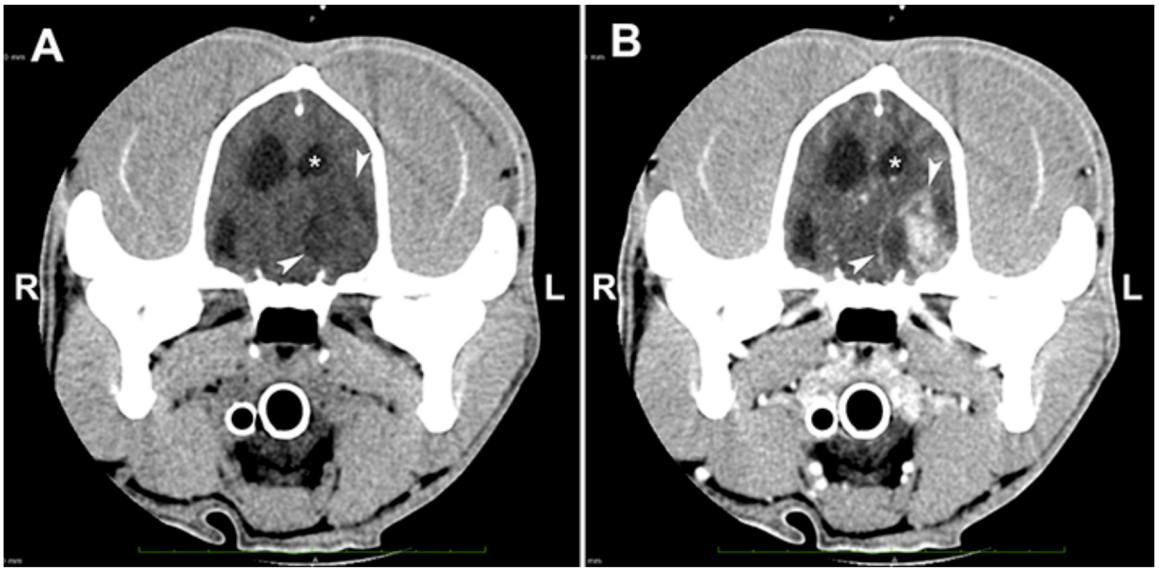

Fig. 10. - Glioma in a 4-years old male Boxer. A) pre-contrast and B) post-contrast transverse scans of the skull at the level of the temporo-mandibular joints. The left parietal-temporal cortex of the brain is slightly hypodense and with a high contrast enhancement (arrowheads). A mass effect is visible to the left lateral ventricle (asterisk).

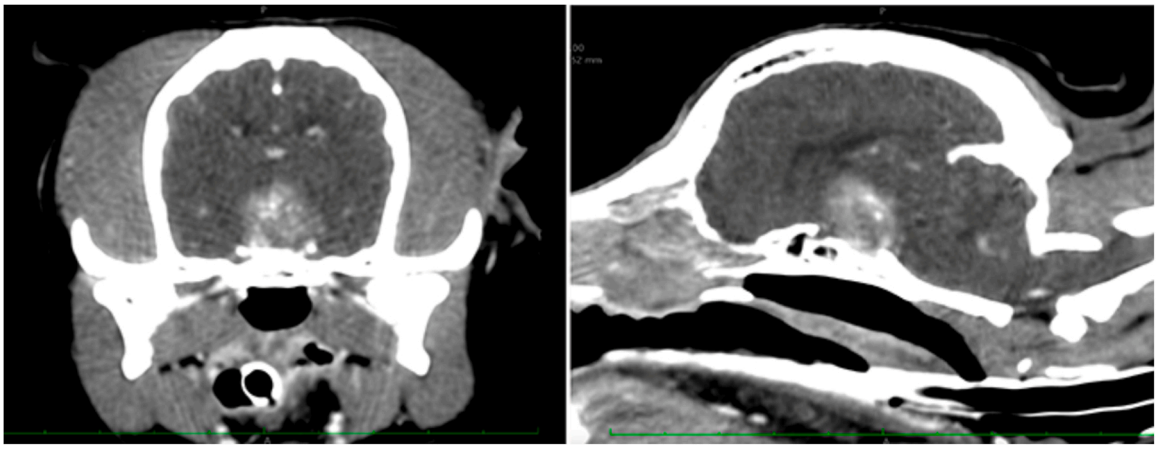

Fig. 11. – Pituitary gland macroadenoma in 13-years old neuterd female Yorkshire terrier. A) transverse scan and B) sagittal MPR post-contrast CT images. On the pituitary fossa, a large and homogeneously contrast enhanced extra-axial mass is visible.

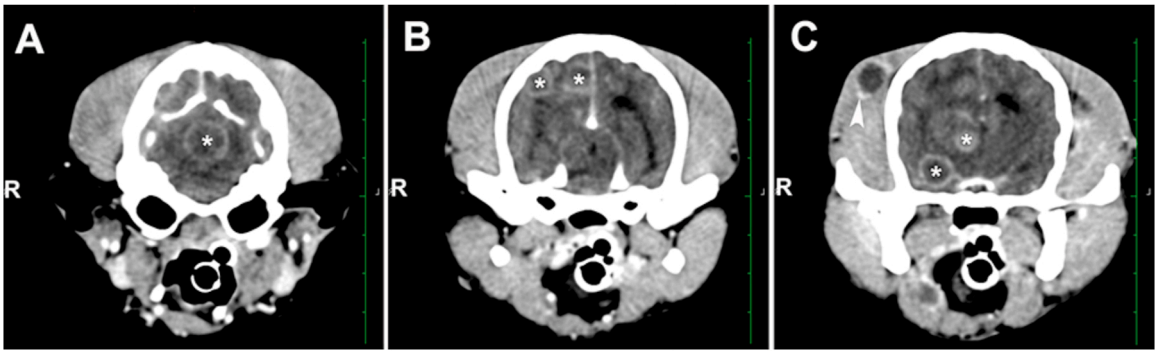

Fig. 12. – Breast cancer metastasis in a 8-years old female mixed breed dog. Post-contrast transverse CT scans at the level of posterior fossa (A) tympanic bullae (B) and temporo-mandibular joints (C). Multiple round nodules of different dimensions and with "ring" enhancement are visible (asterisks). Another metastasis is visible within the right temporal muscle (arrowhead).

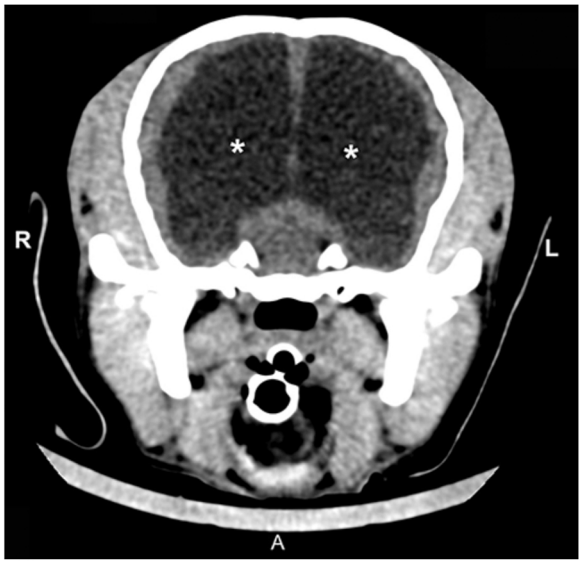

Fig. 13. – Congenital hydrocephalus in an 8-months old male Cavalier King Charles spaniel. Both the lateral ventricles are severely dilated (asterisks). The brain tissue is thin and compressed toward the calvarial bones and the falx cerebri.

oligodendroglioma are quite common in dogs but rare in cats [30]. Choroid plexus tumours are less frequently in dogs and, even if Golden retrievers ore overrepresented, a breed predisposition was not confirmed [32]. Ependymomas, neuronal tumours, microglial tumours, cerebellar medulloblastomas are rare in pets [30]. Gliomas are over-represented in brachycephalic breeds (e.g. Boxer, Boston terrier, Bull-mastiff, English bulldog, and French bulldogs) (Fig. 10) [33]. Computed tomographic features of brain tumours are variable and sometimes common to multiple diseases: they are isodense or hypodense, with a mass effect from mild to severe, due to oedema and lesion itself, characterized by midline shift and ventricular system compression. Contrast enhancement is quite variable depending on the type of disease: it can be weak or strong, homogeneous (uniform) or heterogeneous, solitary, multiple, widespread, with or without ring effect, complete or incomplete [34,35].

Pituitary tumours are generally represented by adenomas (micro and macro) characterized by uniform strong contrast enhancement (Fig. 11) [36].

The most frequent secondary brain tumours are hemangiosarcoma, lymphoma and carcinoma (mammary, prostatic and pulmonary) [3,30]. The presence of multiple nodules with a "ring effect" enhancement is commonly seen in metastatic tumours (Fig. 12) although metastatic carcinoma can also appear also as a single mass.

Hydrocephalus is a common abnormality affecting especially toy breed dogs, brachycephalic dogs and Siamese cats (Fig. 13) [37].

Computed tomography is also used in case of brain vascular

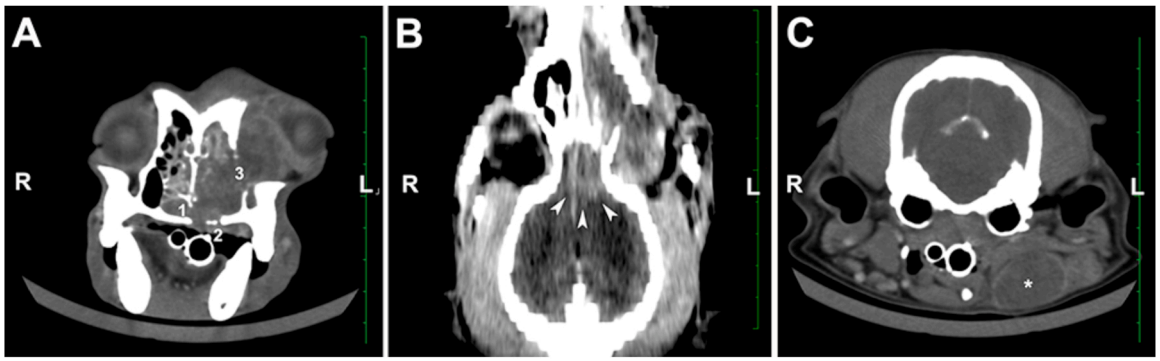

Fig. 14. – Adenocarcinoma of the left nasal cavities in a 12-years old female mixed breed dog. A) transverse post-contrast CT scan at the level of the orbitae; B) Dorsal MPR post-contrast image; C) Transverse post-contrast CT scan at the level of tympanic bullae. A severe bone lysis of the septum (1), the palatine bone (2) and the lacrimal bone (3). The mass invades the retro-orbital space, dislocating dorso-laterally the left eyeball, and the anterior fossa dislocating the olfactory lobes (arrowheads). A metastatic lesion is visible in a mandibular lymph node (asterisk).

Fig. 15. – Chronic right otitis media in a 9-years old male Beagle. Transverse CT scan at the level of tympanic bullae. The right bulla is filled by material isodense to the surrounding soft tissue and a small bone lysis (arrow) and periosteal reaction (arrowheads) are visible.

disorders (i.e. ischemic or haemorrhagic infarction) [38–40]. Inflammatory diseases of the brain are usually challenging to detect using CT. When recognizable, meningoencephalitis is characterized by multifocal slightly hyperdense lesions with homogenous contrast enhancement [41]. In dogs and, rarely, in cats, a granulomatous meningoencephalitis (GME) is described and characterized by focal or disseminated foci, from isodense to hyperdense, with ill-defined contrast enhancement [42].

Computed tomography is the best technique for evaluating nasal neoplasia, generally represented by adenocarcinomas [43]. The pattern includes sclerosis and lysis of the nasal conchae. In severe cases, the neoplasia destroys the nasal, maxillary, palatine, lacrimal, frontal and ethmoidal bones and extends to the ipsilateral retrobulbar space. In some instances, the nasal tumors, after the lysis of the cribriform plate, reaches the anterior fossa of the brain with associated oedema and heterogeneous contrast enhancement (Fig. 14) [44,45]. In cats, previously described features are usually associated with adenocarcinoma and lymphoma, although the destruction of the nasal conchae is less prominent in case of lymphomas [46].

Recently, CT findings of primary and/or secondary retrobulbar space diseases have been described [47,48]. Among primary retrobulbar disorders, the most frequent are neoplastic or septic lesions, including fungal infections in cats [49,50]. Secondary retrobulbar diseases were highly associated with neoplasia [47].

Computed tomography is widely used in small animals to study external, middle and inner ear abnormalities. These are characterized by increased attenuation of the tympanic cavity, thickening and/or lysis of the bulla walls (Fig. 15) [51,52].

1.2. Spine

For the evaluation of the spinal cord and nerve roots diseases, MRI has a higher diagnostic sensitivity. Therefore, CT is preferably used in case of injuries of the spine, due to trauma, congenital bone malformations (Fig. 16), discospondylitis, etc. However, since the shorter time of acquisition and the diffusion in veterinary practice, CT is also used for other pathological conditions such as degenerative diseases of the intervertebral disc in chondrodystrophic dogs. Non-contrast CT, intravenous contrast CT, CT-myelography and positional or dynamic CT have been reported (Fig. 17) [8,53–57]. Computed tomographic findings of intervertebral disc extrusion include hyperattenuating material, usually represented by fragments of the degenerated calcified *nucleus pulposus* within the spinal canal, epidural fat loss, and spinal cord compression (Fig. 18) [53]. Usually, the intervertebral disc extrusion can be demonstrated with non-contrast CT but, if it cannot demonstrate the lesion, CT-myelography can be used (Fig. 19) [55]. After the administration of i.v. contrast medium, enhancement of the compressed tract of the spinal cord could be visible [56].

1.3. Skeleton

Despite the high spatial resolution, in veterinary medicine, CT does not have the same outcomes as in human medicine for assessing osteoarticular abnormalities. Of note, one of the most frequent CT indications is canine elbow dysplasia. This condition is inherited, overrepresented in many large dog breeds and characterized mainly by four diseases: the ulnar medial coronoideal process fragmentation, the ununited anconeal process, the osteochondrosis dissecans of the humeral condyle and the articular incongruence (Fig. 20) [9,58,59]. When radiography is inconsistent, CT is also indicated for the osteochondrosis of the stifle and tarsus. Computed tomography has also been proposed to investigate canine hip dysplasia [10,60,61].

1.4. Thorax

As in humans, CT is considered the second level technique, after radiography, to evaluate thoracic diseases. However, still today, there are no standardized protocols. This lack of standardization is most likely due to several factors that may coexist: type of CT device employed, patient size and its clinical status, the conditions in which the scan is performed (awake vs. anesthetized patient), the administration of the contrast medium (manual vs. automatic injection), etc. [62].

Dogs and cats have a cranial and a caudal lobe on both lungs (the left cranial lobe is divided into cranial and caudal parts by an intralobar

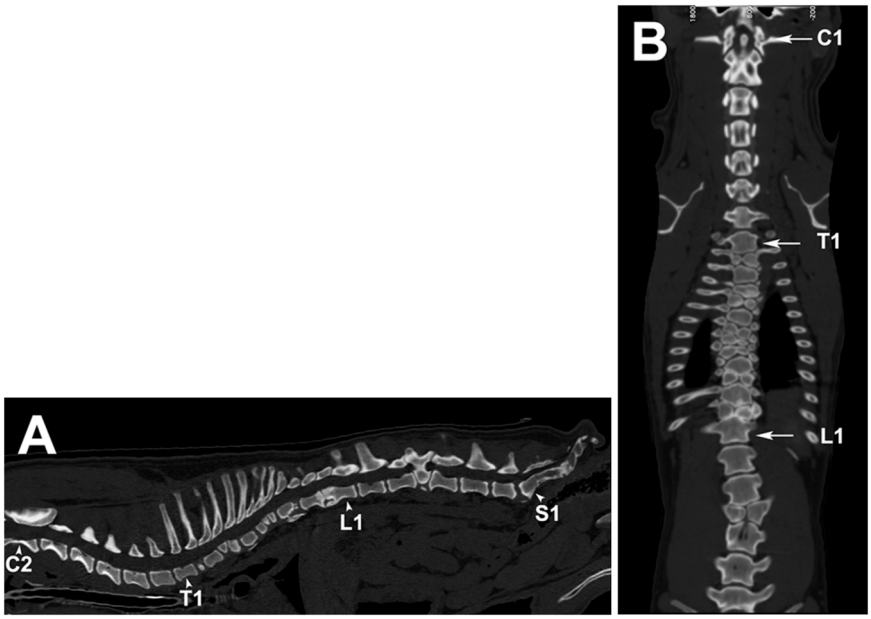

Fig. 16. - Multiple vertebral congenital malformation in a 5-years old female English bulldog. Sagittal (A) and dorsal curve (B) MPR of the vertebral column. Multiple hemivertebrae and "butterfly" vertebrae at the thoraco-lumbar tract are visible. The first vertebra of each tract is marked, in order to identify the malformed vertebrae, considering that vertebral formula in dog and cat is: 7 cervical, 13 thoracic, 7 lumbar and 3 sacral vertebrae.

fissure), a middle (cardiac) and an accessory lobe on the right lung [63]. Regarding the ultrastructural organization, the lung parenchyma in dogs and cats differs from that of humans. In fact, in these animals, the secondary pulmonary lobule is not recognizable [64]; therefore, the terminology used for humans could not fit animals. For these reasons, recently, a new systematic approach for evaluating of the pulmonary parenchymal abnormalities, including three main topics (distribution, lung pattern, and anatomic localization) each divided into subclasses, has been proposed [63].

Computed tomography indications for clinical use in animals are similar to those in human beings, although it is mainly used for cancer patient staging. In dogs, primary lung tumours have a relatively low incidence [65] and usually involve elderly animals. In contrast, breast cancer metastases, from mammary gland carcinoma, are the most frequent neoplastic disease (Fig. 21) [66]. It has been estimated that up to 50 % of female dogs had metastases at clinical presentation [67]. In dogs and cats, CT is also used in thoracic trauma, pulmonary vascular embolic diseases, including infarction, and lung lobe torsion [68]. An important indication of CT, especially in dogs, is the search for vegetable foreign bodies, usually represented by inhaled grass-awn [69].

Computed tomography is also indicated in case of mediastinal masses [70–73]. The most common are lymphoma and thymoma (Fig. 22), while neurogenic, paraspinal, tumor, ectopic thyroid or parathyroid, heart-base tumours and idiopathic mediastinal cysts are rare [74–76].

There are few reports on the use of CT for the study of pleural disorders in dogs and cats [77] and usually circumscribed to pneumothorax and pleural effusion when ultrasonography and radiography are inconsistent. Irregular thickening of parietal pleura, masses and nodular lesions are common findings [78]. In dogs and cats, pleural spaces communicate through several fenestrations. This anatomical features explain why pleural effusion and pneumothorax are often bilateral [78].

1.5. Abdomen

Computed tomography is mainly used for the characterization of large masses or pelvic diseases, where radiography and ultrasonography are usually inconsistent, for assessing their spatial relationships, in case of surgical or radio-therapeutical planning, and for their staging [79].

Hepatocellular carcinoma exhibit a central and marginal contrast enhancement in the arterial phase, while in the portal and late phases is hypoattenuating and cyst-like. Hepatic adenoma shows diffuse contrast enhancement during the arterial and portal phases and isoattenuating during the late phase [80]. Triple-phase CT can provide information to distinguish different focal liver lesions and establish clinical decisions (Fig. 23). Evaluations of the maximal transverse diameter of focal liver lesions and the post-contrast enhancement pattern could predict liver malignancy [81]. Of note, in a study on hepatic lymphoma, the application of CT in suspected cases of hepatic lymphoma, the mean Hounsfiled unit values obtained in all the phases were significantly lower than in the control cases. Furthermore, a periportal "collar sign" was observed in 60 % of the affected patients [82].

Portosystemic communications are relatively common in dogs and cats [82]. Congenital intrahepatic and extrahepatic shunts, arterioportal fistulae, and multiple acquired portosystemic shunts are well recognizable on post-contrast CT (Fig. 24) [83,84]. However, protocols are not always unique and easily repeatable, as they vary according to vascular anomaly, the patient size and the CT scanner used.

Computed tomography is used in dogs to evaluate gastrointestinal diameter and wall thickness [85]. Gastrointestinal tumours are uncommon in dogs and cats [86,87]. Adenocarcinoma exhibits the highest incidence in dogs (Fig. 25), while lymphoma is the most common tumour in cats [88–90]. Gastrointestinal stromal tumours, mast cell tumour (mastocytoma) and fibrosarcoma are rare [87]. Since 40 % of dogs affected by gastrointestinal neoplasia showed metastasis at the diagnosis, CT is reccomended for complete staging [85,90]. Adenocarcinoma appears on CT as a thickening and hyperattenuating wall with strong contrast enhancement. On the other hand, lymphoma is hypoattenuating and exhibits low contrast enhancement [91,92]. Concurrent intra-oral administration of water increases the accuracy of CT in detecting gastric neoplasia [92,93]. Among the non-neoplastic abnormalities, recently, CT has recently been proposed for diagnosing gastrointestinal obstruction in dogs and cats, as it has demonstrated a strong correlation between CT and surgical findings (100%) [94].

Canine pancreatitis is a common and underestimated disease [95,96]. A triple-phase CT study has been recently considered a valuable tool

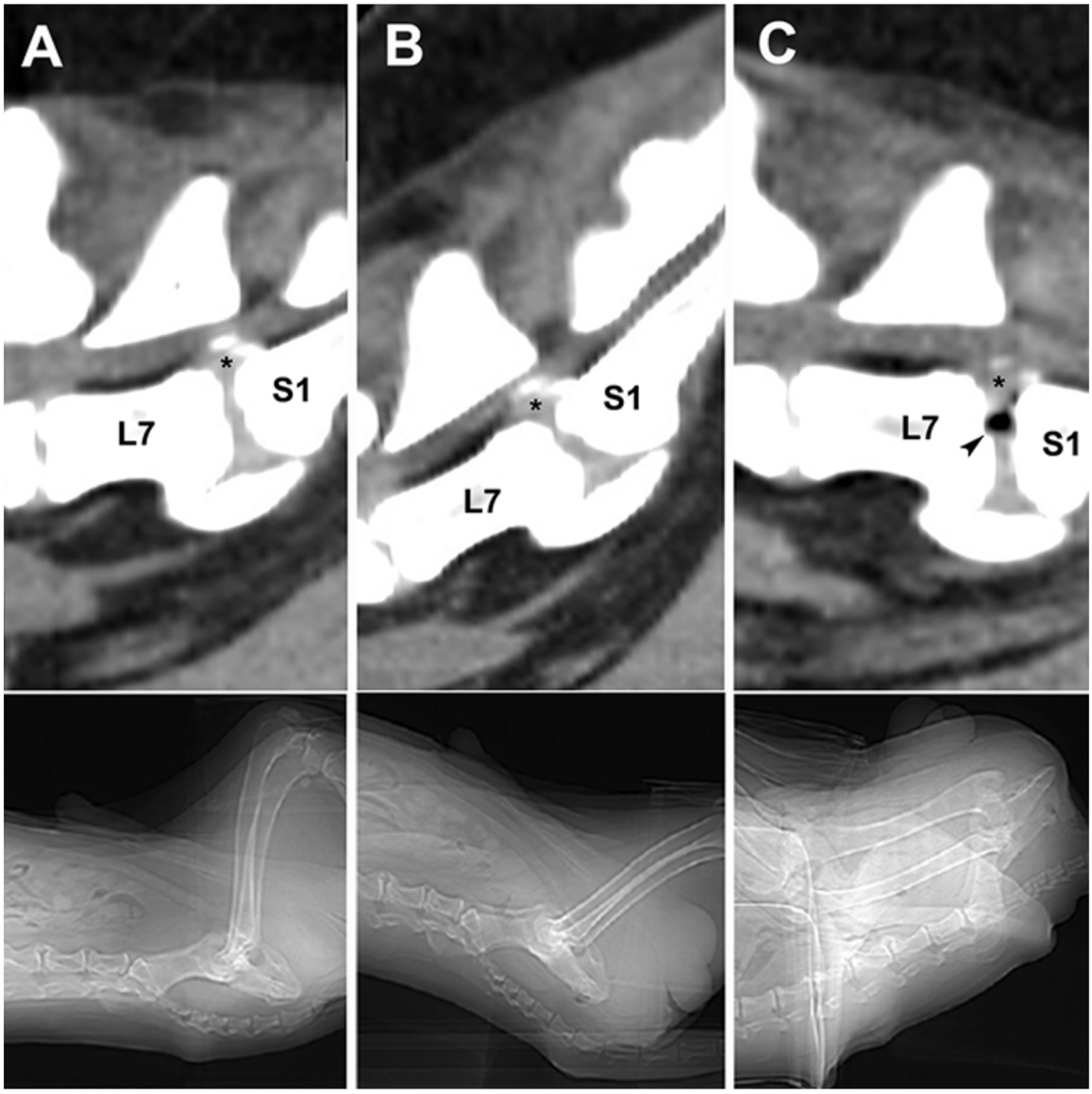

Fig. 17. – Degenerative lumbosacral stenosis in a 7-years old male Beagle. Positional (dynamic) CT: A) Sagittal MPR obtained in neutral position; B) Sagittal MPR obtained in extended position; C) Sagittal MPR obtained in flexed position (at the bottom of each, the respective lateral scout image). The vertebral canal stenosis, due to the protruding and partially mineralized disc (asterisk) gets worse in the extended position while it flattens in flexed position. Notice that in the flexed position, a small vacuum phenomenon appears (arrowhead).

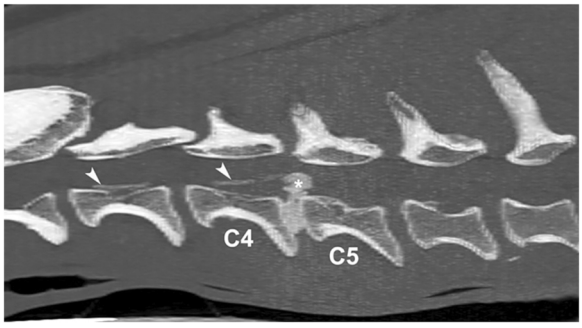

Fig. 18. – C4-C5 acute intervertebral disc herniation (Hansen type I) in a 12-years old male mixed breed dog. The degenerated and mineralized disc (*) is dorsally extruded. The dura mater is partially mineralized (arrowheads) and, close to the lesion, dorsally lifted due to the compression exerted by the herniated disc.

in diagnosing acute pancreatitis in dogs [97]. Portal vein thrombosis, biliary duct dilatation, biliary mineralization, gastrointestinal wall thickening, fat stranding, peritoneal effusion, and lymphadenomegaly have often been associated [97]. Feline pancreatitis was also indagate using radiolabeled leukocytes (99mTc-HMPAO) and computed tomography [98].

The computed tomographic features of adrenal gland disorders, particularly in dogs, are well characterized [99–101]. An excellent correlation between CT findings and surgery or necropsy, in dogs in dogs affected by primary adrenal neoplasia (adenoma, adenocarcinoma and pheochromocytoma), was found (Fig. 26) [102].

Recently, the CT features of focal splenic lesions, which are very common in dogs, were proposed. Marked enlargement and cyst-like appearance with low enhancement are the typical features of splenic sarcomas [103]. Nodular hyperplasia is generally characterized by small and multiple mass of small size, with strong contrast enhancement [3, 104].

The most common renal tumours, renal cell carcinoma, lymphoma

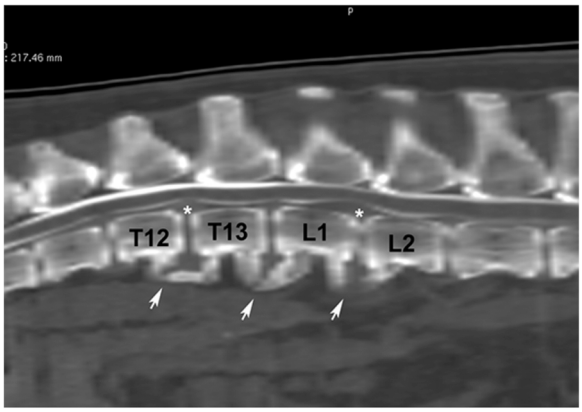

Fig. 19. – Multiple chronic intervertebral disc herniation (Hansen type II) in a 10-years old male German shepherd. Sagittal MPR of CT-myelography. Two intervertebral discs protrusion (asterisks) with a moderate spinal cord compression are visible at level of T12-T13 and L1-L2. The vertebrae are affected also by spondylosis with ventral enthesophytes (arrows).

and hemangiosarcoma, do not significantly differ on CT except for the frequent bilateral presentation of the lymphoma (Fig. 27) [105].

The bolus tracking technique can be used to establish the moment to start the scan for evaluating the uretero-vesicular junction in dogs [106], and 4D-CT excretory urography has been proposed as an accurate and reliable diagnostic technique to investigate canine ureteral ectopia (Fig. 28) [107].

In dogs, CT is indicated for diagnosing and staging different neoplasia of the female genital tract [108]. Ovarian tumours in dogs appear as large soft-tissue masses located in the mid-ventral abdomen, with moderate or marked contrast enhancement [109]. Computed tomographic findings of mesenchymal tumours of the uterus and vagina have recently been described, but except for the greater dimension of malignant neoplasms compared to the benign ones, no other distinctive characteristics have been identified (Fig. 29) [110].

Computed tomography is not widely used to study of the male genital system. Its use is mainly confined to the study of the prostatic gland in the dogs [111]. Recently the prostatic volume in dogs was determined by CT [112]. Finally, CT shows a greater sensitivity compared to ultrasonography in demonstrating inhomogeneity of the prostate gland parenchyma [111].

2. Magnetic resonance imaging

Veterinary institutions started installing their own Magnetic Resonance Imaging (MRI) scanners only in the 1990 s [113] Initially, most veterinary MRI studies involved the dog's head and brain [113–115], and were thereafter employed to investigate spinal and orthopedic pathologies [116].

As well known, MRI scanners are classified into three categories: low-field (0.2–0.4 T), medium-field (0.5–1 T), high-field strength (> 0.1 T) [117]. High-field systems improve the quality of images. They are preferred for studying the brain, and permit the application of advanced sequences. Unfortunately, those systems have high costs for purchasing, running and maintenance. The low-field MRI open scanners are the most diffuse in Veterinary practice for their low cost, ease of installation and maintenance [117,118]. Veterinary systems tend to be cheaper and offer vet-specific software. They have coils optimized for veterinary anatomy but feature lower technology standards.

The main disadvantage of low-field MRI is a lower signal-to-noise ratio (SNR) compared to high-field devices. This disadvantage leads to lower spatial and temporal resolution (i.e. longer acquisition times). For some conditions, such as meniscal tears in dogs, high-field imaging appears to work better than low-field imaging with regard to sensitivity [118]. Therefore, due to the low SNR, it can be challenging to obtain diagnostic studies of the spine, particularly in small patients [117] Additionally, imaging of the caudal cervical or cranial thoracic spine may not be possible in larger dogs [118].

Conventional MRI-compatible anesthesia and monitoring equipment are used in veterinary MRI. For the preparation of the patient, Veterinary MRI studies require, beyond general anesthesia, the removal of metallic objects (e.g. collars, tags, etc.). Microchips implanted near the cervical spine or the brain are usually associated to susceptibility artifacts. However, no malfunctioning of devices is generally observed using MRI from 0,5–3 T. Straight positioning of the patient in sternal or dorsal recumbency is generally required for brain MRI. After the localizers plans, a slice thickness of 3–4 mm is ideal for small animal MRI [115, 117,118].

Chemical displacement artifacts, susceptibility artifacts, and motion /current artifacts are reduced or less noticeable with low-field imaging. The small field of view of the low-field units may require repeated

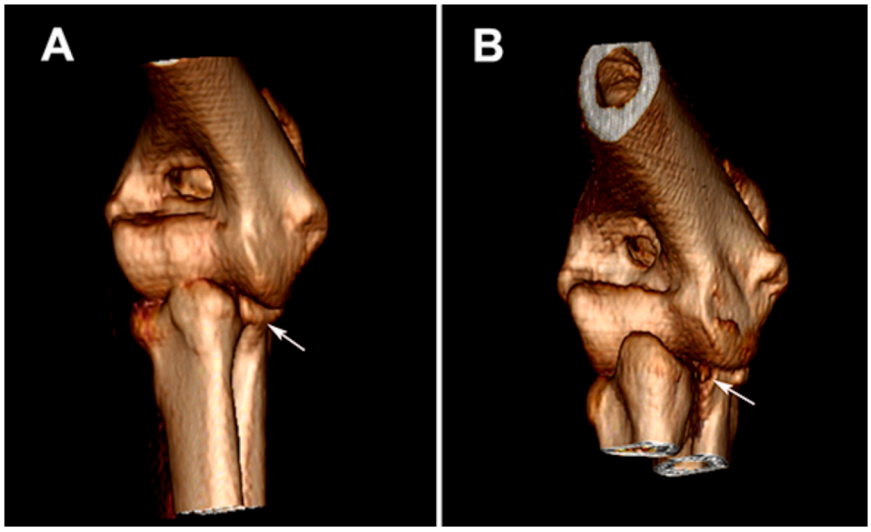

Fig. 20. – Normal (A) and fragmented medial coronoid process (B) of the ulna. 3D volume rendering images. The ulnar medial coronoid process (arrows) is clearly fragmented in the elbow imaged in B.

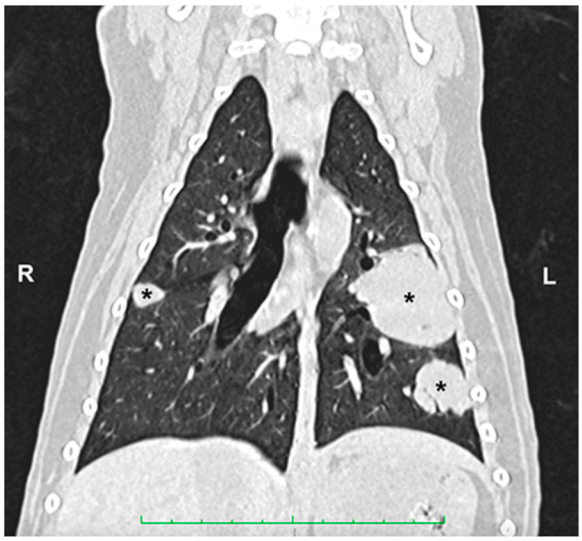

Fig. 21. – Breast cancer metastasis in a 15-years old female Pug. High-resolution dorsal MPR CT. Three regularly shaped lung nodules (asterisks) with different dimensions are visible.

patient repositioning to obtain images of the entire region of interest, particularly for the thoracolumbar spine [117,118] Furthermore, the difference in processional frequency between fat and water is too small in low-field MRI to allow selective chemical saturation (spectral suppression of fat), so this method cannot be used [118]. Of note, the visibility of gadolinium-enhanced lesions is lower with low-field imaging, and some authors have proposed increasing the gadolinium dose when using low-field scanners to compensate for this relatively reduced visibility. Low SNR in low-field systems can, to some extent, be compensated by increasing the slice thickness, reducing the resolution of the plan, increasing the number of acquisitions and, finally, decreasing the bandwidth. These adjustments reduce image resolution, image acquisition time and, consequentely, anesthesia duration time that, potentially, can lead to patient's hypothermia [117,118].

Despite in Human medicine, where the use of gadolinium is correlated to adverse effects related to the renal function, in Veterinary medicine there are only a few reports about anaphylactoid reactions [119]. Consequentely, the administration of contrast agents is encouraged, especially in patients with chronic neurological signs. Clinicians have no agreement regarding the exact timing for the MRI acquisition after contrast media administration. Usually, images are acquired immediately post-contrast injection, while in some conditions, images are obtained in a more delayed phase [120,121].

In dogs and cats, MRI is mainly used for assessing the CNS, while in athlete horses it is mainly used for the appendicular muscolo-skeletal system.

Neverthless, in Veterinary medicine, MRI has become the technique of choice to evaluate brain parenchyma [122–124]. Clinical signs such as seizures, ataxia, cranial nerve abnormalities, paresis, and paralysis are indications for using MRI. The administratin of Gd-DTPA during intracranial imaging could highlight damage to the blood–brain barrier [122]. Intracranial structures that lack a blood–brain barrier, including the choroid plexus, pituitary gland, infundibulum, dura mater, cavernous sinuses, cortical veins, and sinus mucosa, will be ever well visible [123,125]. Magnetic Resonance Imaging can also depict inflammatory and other non-neoplastic conditions of the CNS as meningoencephalitis caused by viruses (Fig. 30) (e.g., distemper), bacteria, or fungi (e.g., cryptococcosis), granulomatous meningoencephalitis in dogs [126,127], necrotizing encephalitis [128], and in the presumptive diagnosis of neurocysticercosis [129].

Haemorrhage of the CNS can be assessed by MRI [130]. T1- and T2-weighted images are necessary to characterize and stage the hemorrhage. Cerebral infarction can also be diagnosed using MRI [131,132]. Metabolic and degenerative hepatic encephalopathy results from severe liver dysfunction or portosystemic shunt (PSS) (Fig. 31). Deposition of manganese in the basal ganglia with hyperintensity on T1-weighted images, brain atrophy and cerebral edema are observed. These brain MRI findings may help distinguish neurological disorders associated with liver disease (including PSS) from other neurological disorders [132,135].

In case of CNS tumors MRI is a valuable tool in their diagnosis. Indeed, MRI can show the primary mass and the extent of any surrounding brain edema. As previously reported, meningioma (Fig. 32), astrocytoma, oligodendroglioma, ependymoma, mixed glioma, dermoid cyst, choroid plexus papilloma, carcinoma and meningeal carcinomatosis are the most common brain tumors in dogs and cats. [133,134, 136].

Intervertebral disc herniation (IVDH) is the most common cause of paralysis in dogs (Fig. 33 and Fig. 34), and MRI is considered the gold standard for imaging the intervertebral disc disease. Of note, the different chemical characteristics of tissues allow distinguishing multiple anatomical structures within the vertebral column (i.e. the

Fig. 22. – Timoma in a 8-years old neutered male Dwarf rabbit. Dorsal MPR post-contrast CT. The cranial mediastinum is occupied by a mass (asterisks) poorly enhanced. Legend: 1 = heart; 2 = lungs; 3 = liver; 4 = right kidney; 5 = left kidney; 6 = spleen; 7 = caudal vena cava.

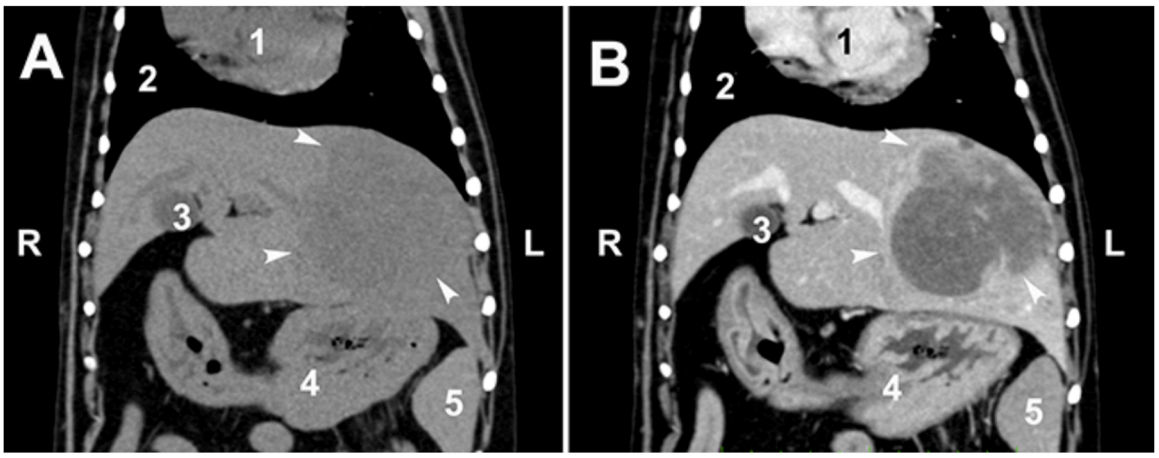

Fig. 23. = Hepatocarcinoma in a 13-years old neutered male Mixed breed dog. Dorsal MPR of pre-contrast (A) and post-contrast (B) CT. In the left hepatic lobes, a large slightly hypodense mass is visible with a post-contrast irregular enhancement, mainly peripheral (arrowheads). Legend = 1 = heart; 2 = lungs; 3 = gallbladder; 4 = stomach; 5 = spleen.

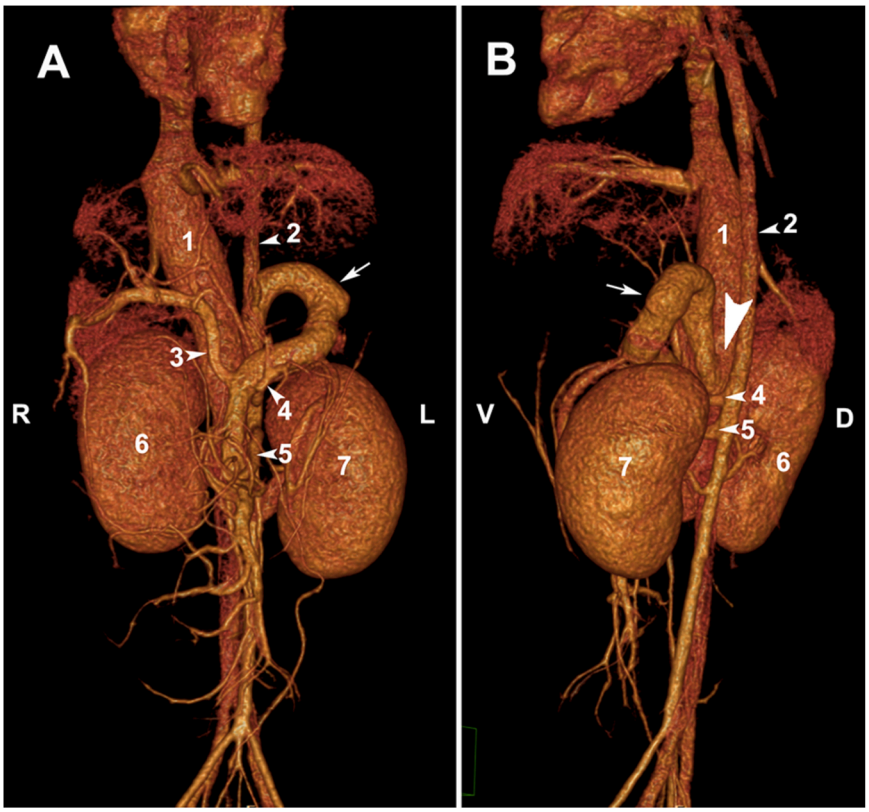

Fig. 24. – Extra-hepatic left porto-caval shunt in a 1.5-years old female Yorkshire terrier. 3D Volume Rendering CT-angiography. A) Ventral aspect. B) Left lateral aspect. A large and tortuous shunting vessel (arrows), starting from the portal vein, travels toward the left and connects to the left side of enlarged caudal vena cava (arrowhead) just cranial to the celiac artery emerging from the abdominal aorta. Legend: 1 = caudal vena cava; 2 = abdominal aorta; 3 = portal vein; 4 = celiac artery; 5 = cranial mesenteric artery; 6 = right kidney; 7 = left kidney.

intervertebral disc, ligamentous structures, synovial joints, bone marrow, nerve roots, spinal cord parenchyma, cerebrospinal fluid, epidural fat). Images can be acquired in multiple planes without repositioning the patient,but the examination is more time consuming than CT. On the other hand, whereas myelography might be required in conjunction with CT, this is not necessary with MRI [137].

Magnetic Resonance Imaging is considered superior to CT for studying the eyeball, the optic nerve and the optic chiasm. Magnetic Resonance Imaging clearly visualizes the palpebral region, the anterior and posterior segments of the eye, the retrobulbar structures, and the zygomatic salivary glands [137]. Abnormalities of the optic nerve, such as optic neuritis, are readily identified. Due to the large amount of fat in the orbital region, MRI fat-suppression sequences, such as Short Tau Inversion Recovery (STIR), are particularly useful to demonstrating the extent of an orbital neoplasms [138,139].

Magnetic Resonance Imaging is complementary to CT or radiography to evaluate the non-osseous components of the shoulder, elbow and knee joints. However, MRI has been used to assess the extent and severity of inflammatory changes within the subchondral bone in dogs with shoulder osteochondrosis (OCD) [140]. Furthermore, MRI demonstrated to be more accurate than radiography in detecting small fragments and cartilaginous flaps (joint mice) within shoulder joint in case of OCD and can provide diagnostic images in canine elbow dysplasia [140]. Regarding the stifle joint, MRI was useful in detecting changes in the cartilage thickness, osteophytosis, and intra-articular loose bodies in experimental osteoarthritis in dogs [141,142]. Magnetic Resonance

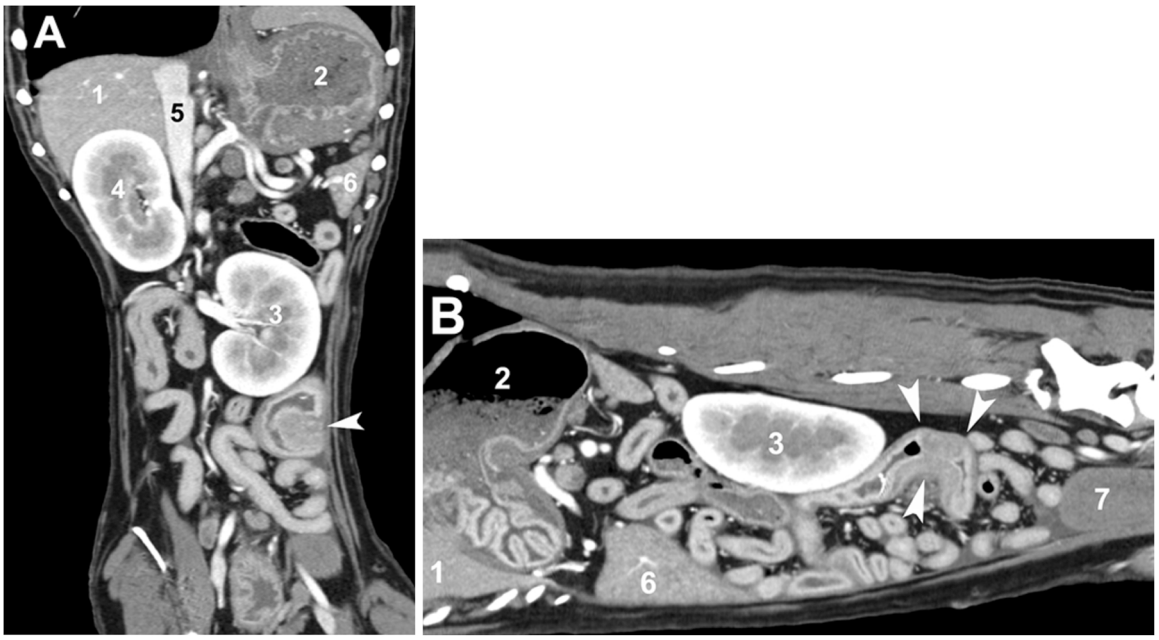

Fig. 25. – Jejunal carcinoma in a 9.5-years old male Siberian husky. A) Dorsal MPR post-contrast CT. B) Left para-sagittal MPR post-contrast CT. Caudally to the left kidney, a short jejunal tract, with circumferential and asymmetrical thickening of the walls, is visible (arrowheads). Legend: 1 = liver; 2 = stomach; 3 = left kidney; 4 = right kidney; 5 = caudal vena cava; 6 = spleen; 7 = urinary bladder.

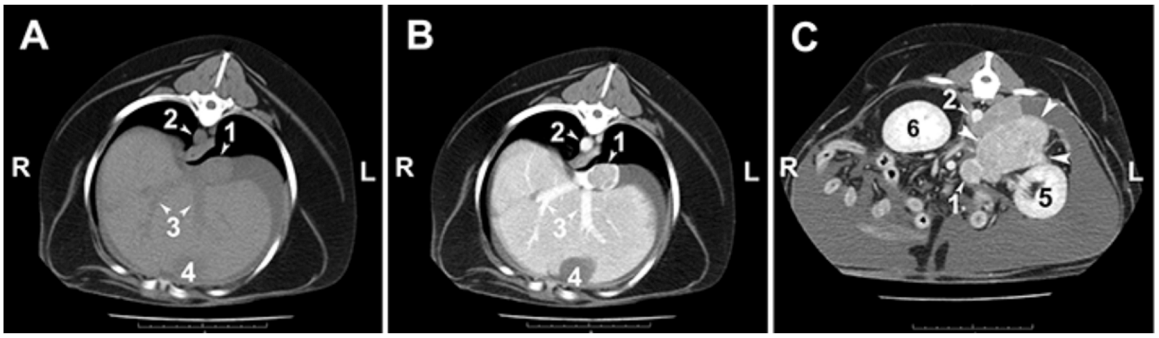

Fig. 26. – Right adrenal carcinoma in a 9-years old male Mixed breed dog. A) pre-contrast and B) post-contrast transverse CT scans of the liver at the level of the 9th thoracic vertebra. C) post-contrast transverse CT scan at level of 11th thoracic vertebra. The lumen of caudal vena cava is invaded by a fairly enhancing thrombus directly originating from the severely enlarged right adrenal gland (arrowheads). Legend: 1 = caudal vena cava; 2 = aorta; 3 = suprahepatic veins; 4 = gallbladder; 5 = right kidney; 6 = left kidney.

Imaging showed cranial cruciate ligament injury in dogs with no or minimal cranial drawer signs [142,143]. The normal MRI anatomy of the canine stifle [143] and carpal ligaments has also been described [144].

MRI plays a key role in studying the musculoskeletal system of the athlete horses. It is used as a third-level technique to supplement the information obtained with radiography and ultrasonography [145]. Magnetic Resonance Imaging allows visualizing soft tissues, tendons, and ligaments, even those in the hoof. Furthermore, it provides image scans in different anatomic planes without repositioning the horse. This feature has allowed significant progress in the diagnostic and therapeutic field, particularly regarding foot pathologies.

The main pathologies diagnosed in athlete horses are tendinopathies of the deep digital flexor tendon, degenerative arthropathies of the distal interphalangeal joint, lesions of the sagittal throat of the proximal phalanx, enthesopathies and desmopathies of the suspensor ligament of the fetlock [146].

Until a few years ago, MRI in horses had to be performed in general anesthesia and in lateral recumbency. Recently, MRI devices that can scan the foot, fetlock, knee or hock of sedated horses in standing position have been developed [146].

In conclusion, MRI is the modality of choice for diagnosing brain diseases in dogs and cats and for chronic foot lameness in horses. The main advantage of MRI is related to the excellent soft tissue contrast useful for distinguishing between white and grey matter or articular structures (cartilage, ligaments, menisci). It has a high sensitivity since most pathologies confer tissue modifications (inflammation, edema, etc.). Moreover, MRI does not use ionizing radiations, unlike radiography and CT. The disadvantages are mainly related to the duration of the sequences: the veterinary magnetic resonance examination can have a variable duration (up to two hours) depending on the number of sequences to be acquired and the body regions under investigation. Furthermore, paient preparation, especially horses, could require several hours.

3. Nuclear medicine

Nuclear Medicine (NM) imaging techniques are not frequently used in Veterinary Medicine because they have high costs and heavy regulations. However, the most used NM imaging techniques are

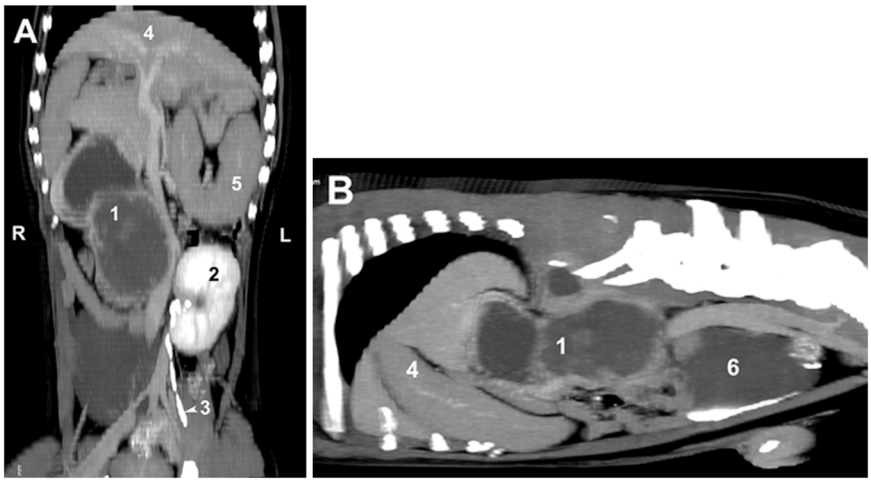

Fig. 27. – Right renal carcinoma in an 8- years old male Boxer. A) Dorsal MIP post-contrast CT. B) Right para-sagittal MIP post-contrast CT. The right kidney is markedly enlarged with a "hour-glass" shape, mainly peripheral and irregularly enhanced, with a central septum. Legend: 1 = right kidney; 2 = left kidney; 3 = left ureter; 4 = liver; 5 = spleen; 6 = urinary bladder.

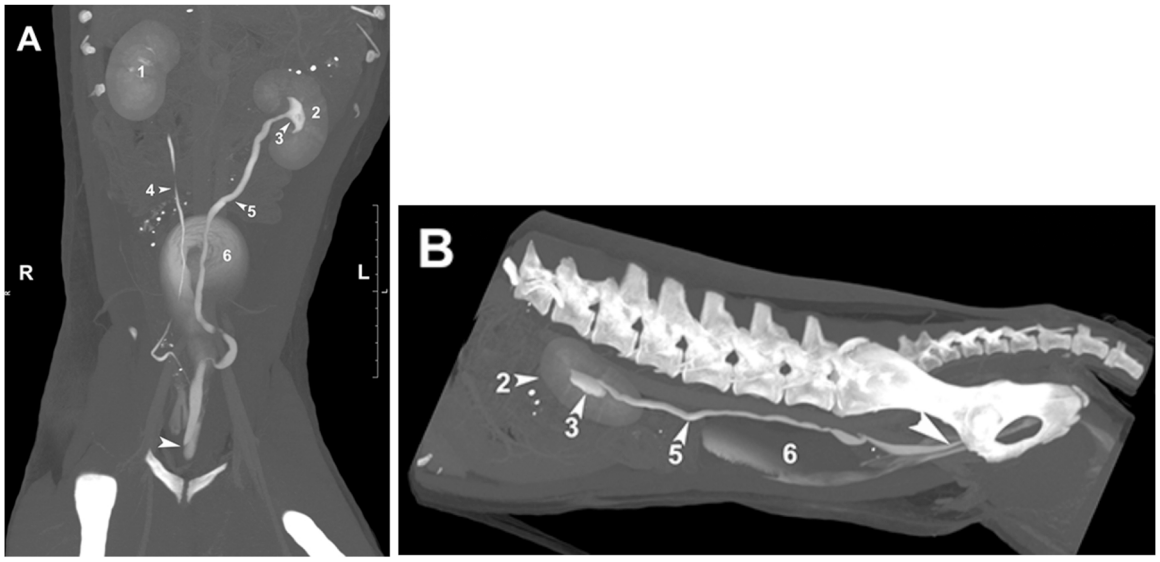

Fig. 28. – Right ureteral ectopia in a 7-months old female Labrador. A) Dorsal MIP post-contrast CT. B) Left para-sagittal MIP post-contrast CT. The left ureter is slightly dilated, as well as the left renal pelvis, and ends caudally to the urinary bladder within the urethra (arrowhead). Legend: 1 = right kidney; 2 = left kidney; 3 = dilated left renal pelvis; 4 = normal right ureter; 5 = dilated left ureter; 6 = urinary bladder.

Scintigraphy and the Positron Emission Tomography (PET), this last often combined with Computed Tomography (CT) [147]. The usefulness of NM techniques is related to the possibility of making an early diagnosis. Still, due to the functional quality of their images, they should be performed combined with other morphologic modalities such as CT or MRI. Unfortunately, this is not always achievable in veterinary practice [148–150].

Scintigraphic images are not morphological but represent physiological or pathological processes of the body that other diagnostic techniques cannot provide. Therefore, they are difficult to interpret for most of clinicians. Access to the radiotracers is high costs and requires a radioactive materials license not always easy to achieve in small animal practice [149]. Furthermore, specific training is necessary for correctly interpreting the images [149].

In veterinary scintigraphy, the metastable Technetium-99 ($^{99\,m}$Tc) is the most used radionuclide, although radioisotopes of Iodium, Indium and Thallium are used in specific instances [150,151]. Radioisotopes can be administered orally, trough injection or by inhalation. It is possible to perform a static or a dynamic studies to follow radiotracer biodistribution over time, following its affinity.

In small animals, scintigraphy is mainly used for oncological problems or to diagnose portal shunts. In athlete horses, the most common use of scintigraphy is for muscoloskeletal pathologies [152,153].

Thyroidal scintigraphy was one of the first used in Veterinary Medicine and it remains one of the most common scintigraphic study. Thyroidal scintigraphy is mainly used to treat feline hyperthyroidism, the most common endocrine disease of the cat. However, it is also used to diagnose thyroid carcinoma and evaluate hypothyroidism in dogs.

Cat hyperthyroidism is secondary to adenomatous hyperplasia, usually of both thyroid lobes or rarely with a unilateral involvement (Fig. 35). Radioiodine administered as a subcutaneous injection represents an easy and effective treatment for feline hyperthyroidism [150, 151].

Thyroid scintigraphy performed using pertechnetate or radioiodine is characterized by a uniform distribution of radioactivity throughout both lobes of the thyroid gland. Traditionally, thyroid imaging is

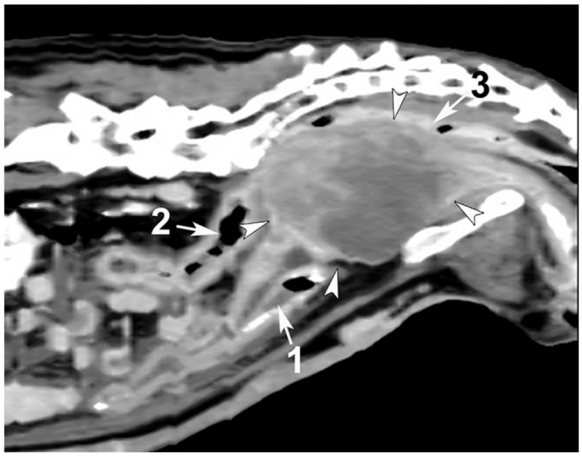

Fig. 29. – Uterine and cervix uteri hemangiosarcoma in a 10-years old female chow. Sagittal MPR post-contrast CT. A large mass involving the body and the cervix of the uterus (arrowheads) with a discrete and irregular enhancement and severe mass effect on the colon and the rectum. Legend: 1 = urinary bladder; 2 = caudal colon; 3 = rectum.

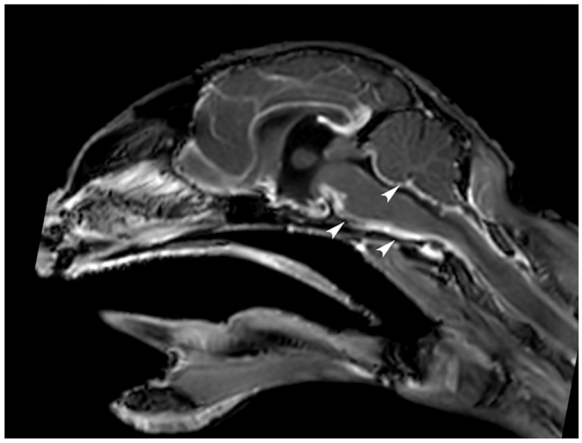

Fig. 30. - Meningitis and meningomyelitis secondary to FIP in a young cat. T1-weighted post-contrast MRI sagittal images. Severe thickening and increased enhancement of the meninges, mainly around the ventral border of the cerebellum, the pons and the medulla oblongata (arrowheads).

performed 20 min after pertechnetate injection. Some Authors have recommended imaging an hour after injection [151]. Unlike human patients, animals have to be hospitalized for one week after the scintigraphic exam to avoid radiation exposure to their owner. After this period, in cat scintigraphy, a further two-week isolation is recommended to limit adults exposure to up to twenty per day. Thyroid scintigraphy can hardly distinguish between hyperthyroidism and thyroid carcinoma. Certainly, in the latter there is usually a higher radioactive uptake. Furthermore, due to associated multifocal lesions, there is an irregular pattern and, often, foci of uptake outside the thyroid lobes, indicating the presence of metastasis. The concomitant use of CT facilitates te detection of intrathoracic metastasis.

It is essential to avoid the use of iodine CT or radiographic contrast agents when performing a schintigraphy in dogs and cats because the iodine contrast agents interfere with thyroid uptake. Dog with hypothyroidism usually displays a low thyroid uptake [151].

The Bone Scan is a great resource for diagnosing obscure lameness issues and localizing orthopedic conditions in horses (Fig. 36), such as bone microfractures, joint inflammation and osteoarthritis (Fig. 37).

The patient is injected diphosphonate bound to radionuclide, $^{99\,m}$Technetium, which is then distributed throughout the body over two hours. The radioisotope is localized in bone based on osteoblastic activity and therefore is an excellent and sensitive marker of bone disease. The bone that is stressed or is remodeling, due to an injury, will absorb a disproportionate amount of the radioisotope. The portions of involved bone will then appear as an area of increased radioisotope uptake, or a "hot spot", on the gamma camera (Fig. 37). The use of the bone scan to diagnose horse lameness is controversial. A recent study demonstrated that scintigraphy is more useful when used combined with other imaging techniques. The high potential for missed diagnoses makes skeletal scintigraphy unreliable as a diagnostic screening tool for sports or pleasure horses with lameness or poor performance [152,153]. Those authors assessed a high proportion of false-negative and false-incidental results and that scintigraphy has a poor sensitivity in identifying the lesion causing lameness in poor-performing athlete horses. They suggest the use in athlete horses after proper clinical investigation and loco-regional anesthesia [152].

Interestingly, scintigraphy with intraosseous injection of technetium $^{99\,m}$Tc pertechnate labelled to allogenic mesenchymal stem cells has been used to safely track allogenic mesenchymal stem cells in healthy and diseased horses [153].

One of the most common veterinary applications of liver scintigraphy is the diagnosis of congenital or acquired porto-systemic shunts (PSSs). The diagnosis of PSSs is achieved with trans-splenic portal scintigraphy (also called portal scan). To date this technique, in small animals, involves the use of $^{99\,m}$Tc pertechnetate or $^{99\,m}$Tc-Mebrofenin. It is essential to distinguish between congenital and acquired shunt because the last one is treated preferably with medical treatment [154].

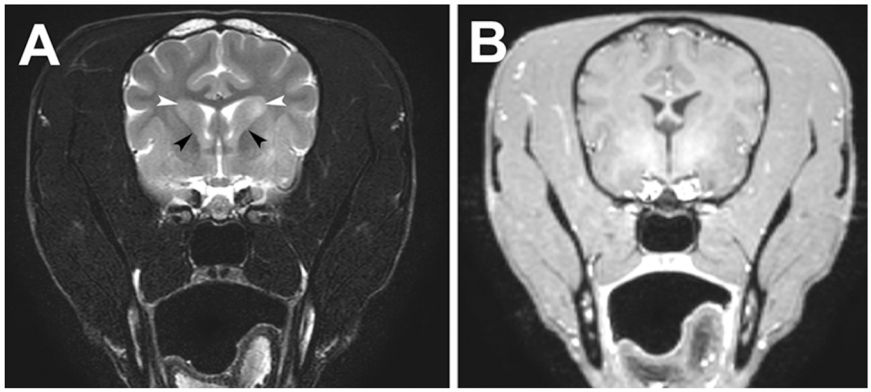

Fig. 31. - Hepatic encephalopathy in an adult dog. T2-weighted (A) and T1-weighted post-contrast (B) MRI transverse images. There is a discrete increased signal intensity in the caudate nuclei (white arrowheds) and internal capsula (black arrowheads). No contrast enhancement is visible.

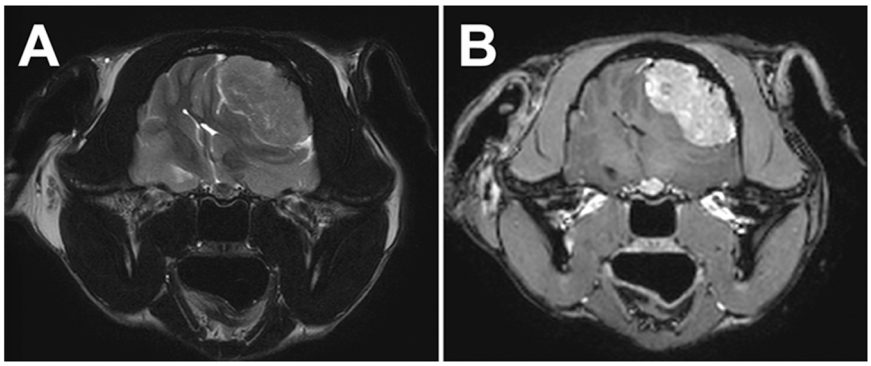

Fig. 32. – Meningioma in an adult cat. T2-weighted (A) and T1-weighted post contrast (B) MRI transverse images. A large extra-axial space occupying lesion, broad based at the level of the left temporal and parietal lobes, is visible. The lesion has an overall hyperintense, slightly heterogeneous enhancement. There is severe mass effect with midline shift, compression and dislocation of the lateral ventricles and deformation of the white and gray matter surrounding the lesion.

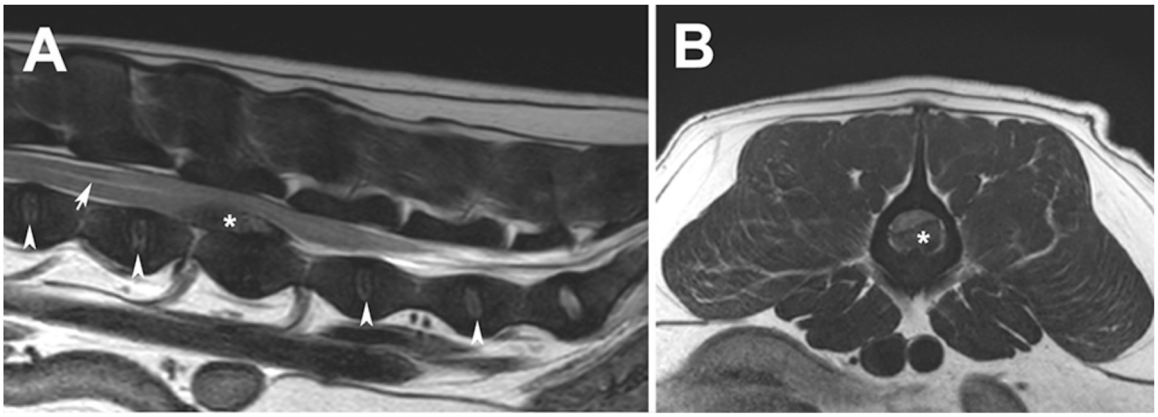

Fig. 33. – Acute disc herniation (Hansen type I) at L4-L5 in an adult dog. T2-weighted MRI sagittal (A) and transverse (B) images. In the spinal canal, a discrete amount of disc material, with heterogeneous signal intensity, causes a severe left ventro-lateral spinal cord compression (asterisk). Cranial to it, there is a slight dilation of the ependymal canal (arrow). Multiple degenerated discs with loss of the normal signal intensity of the nucleus pulposus are visible too (arrowheads).

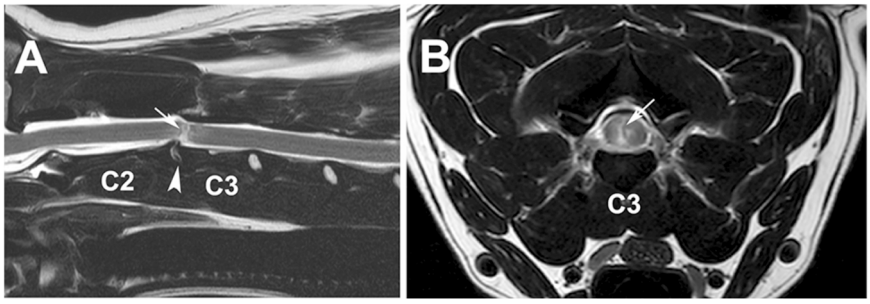

Fig. 34. – Low-volume-high-velocity disc herniation at C2-C3 in an adult dog. T2-weighted MRI sagittal (A) and transverse (B) images. It is visible a degenerated disc with partial loss of the normal signal intensity of the nucleus pulposus (arrowhead), and a hyperintense tract through the annulus fiibrosus that continues as a linear and marked hyperintensity into the spinal cord dorsal to it (arrows), that is compatible with spinal contusion.

Per-rectal scintigraphy technique with ^{131}I-iodoamphetamine (^{131}IMP), has the disadvantages of high cost and longer half-life of radiotracer [155]. To date, pertechnetate is preferred, even per-rectal, since the shorter half-life, lower cost, ready availability, unchanged absorption and ideal photon energy [156]. Because of some limitation regarding the absorption, the high dose needed, the exposition and the poor differentiation between the intra- and extra- hepatic shunts, other imaging techniques, such as CT, are often required. The trans-splenic portal scintigraphy is performed by administrating a small dose of radioisotope into the spleen under ultrasound guidance [157]. The passage of the radioisotope is evaluated in real-time to determine if a macroscopic shunt is present and if the pattern of uptake supports a single congenital shunt or multiple acquired shunts. An abdominal CT often accompanies this procedure to evaluate the intra-abdominal organs further and better delineate the shunting vessel(s). Trans-splenic portal scintigraphy can also be performed with $^{99\,m}$Tc-mebrofenin, which has higher absorption, a better morphologic evaluation and no complications [157–159]. The use of $^{99\,m}$Tc-mebrofenin also reduced the proportion of non-diagnostic studies. Today, for diagnosing PSSs, Doppler ultrasonography is considered the first imaging technique, followed by CT angiography and, eventually, scintigraphy.

Positron Emission Tomography (PET) and Single photon emission computed tomography (SPECT) are widely used in human medicine for the detection and staging of many diseases, particularly for the detection

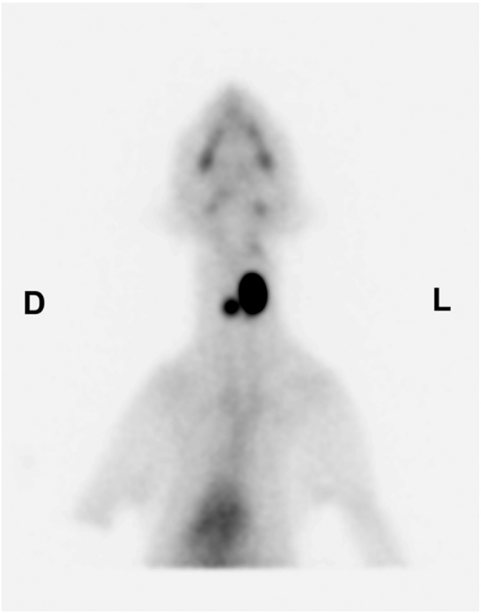

Fig. 35. - Bilateral thyroid adenoma. $^{22\,m}$Tc- pertechnetate thyroid scintigraphy in an adult cat. Ventro-dorsal projection. There is a marked uptake in both thyroid lobes, but more evident in the left one. No ectopic thyroid tissues are detectable.

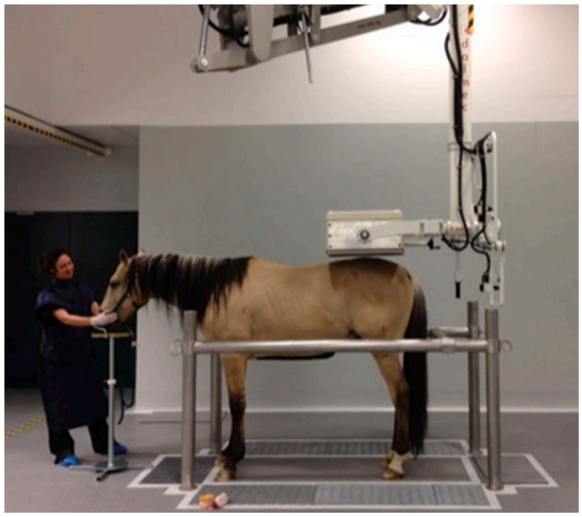

Fig. 36. - Bone scan on a sedated horse in standing position undergoing to pelvis and sacroiliac joints study.

of primary tumors and metastasis but also for the diagnosis of neurodegenerative diseases. Those techniques are even more sensitive than the morphological techniques in the early detection of many diseases. However, they are often combined with CT or Magnetic Resonance (MRI) to provide morphological reference points to the PET or SPECT functional images [160].

One of the most used radiotracers in human medicine is Fluorine 18 fluorodeoxyglucose (^{18}F-FDG), a glucose analogue up taken by cells with high metabolic activity, like the heart, brain, inflammation cells and cancer cells [161,162].

Like in Human Medicine, in veterinary medicine ^{18}F-FDG PET/CT has been used for staging mammary adenocarcinoma, lung tumors, lymphoma, gastrointestinal stromal tumor, histiocytic sarcoma [162], splenic hemangiosarcoma [163], feline oral squamous cell carcinoma [164] and canine oral melanoma [165].

In a study on dogs with appendicular osteosarcoma, the authors correlated the Standardized Uptake Value to the progression of the cancer for assessing dogs' survival [166]. PET is also more advantageous than CT in detecting hypervascularized tumor areas. Indeed, PET highlights areas with higher metabolic activity, while contrast-enhanced CT highlights areas of increased perfusion. Furthermore, CT cannot distinguish between increased tumor blood perfusion and highly vascularized tumor background.

^{18}F-Sodium Fluoride (^{18}F-NaF) has proven to be an excellent osseous tracer, and it is used to assess primary bone tumors or bone metastasis. This tracer has an interesting role in staging canine nasal adenocarcinoma [167]. Recently, Manfredi et al. demonstrated the usefulness of preoperative scintigraphy with Technetium-99 m labelled nanocolloids for detecting the sentinel lymph node and the associated lymphatic pathway in dogs with spontaneous malignancies (Fig. 22) [168].

However, the use of PET/CT in evaluating non-oncologic small animals is still limited. Few reports have been available since now. ^{18}F-NaF has been used to diagnose dog lameness [169,170] and to assess temporomandibular joint disorders [170], as well as for active bone remodelling in horses [171–174].

SPECT imaging is relatively unused in Veterinary medicine. First, this technique always requires general anesthesia. Second, it is necessity to have gamma cameras suitable for both horses and small animals. Finally, species-related software is necessary. SPECT imaging is widely used in Human medicine to diagnose heart ischemia, but this pathology is rare in small animals. Furthermore, in Veterinary medicine there is not a great interest about the study of neuroreceptors, or brain perfusion, thus raising the main interest of SPECT: the study of neurological diseases [139–175]. Fig. 38.

SPECT has been used in Veterinary Medicine for the diagnosis of thyroid carcinoma and to screen thoracic metastasis in the dog (Fig. 39) [176,177]. Due to owners' increasing interest in studying of the owners on studying their dogs' behavior, SPECT with ^{123}I-FP-CIT is widely used for in vivo assessment of the dopamine transporter (DAT) availability. Alterations in dopamine are associated with behavioral disturbances in

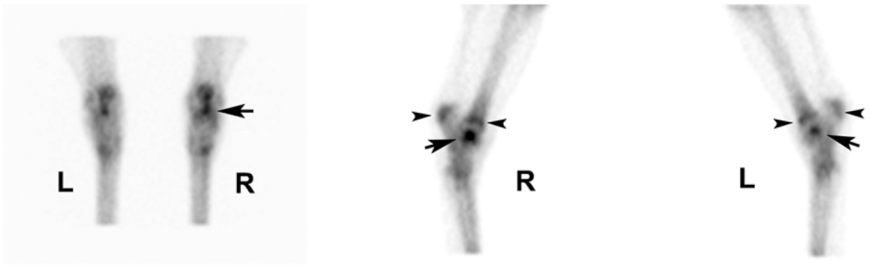

Fig. 37. - Osteocondrosis of the astragali in a foal. Planar bone scan in plantar, right and left lateral images of the hock region. There is an increased focal uptake of the subchondral bone of the astragali (arrows) more pronounced to the right. A discrete uptake is visible also at the level of epiphyseal growth cartilages of the distal tibia and the top of calcaneus (arrowheads).

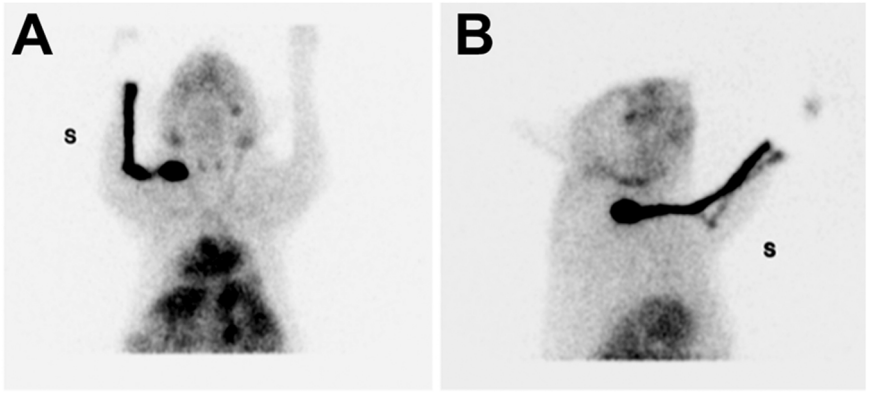

Fig. 38. – Lymph scintigraphy in a French bulldog with mastocytoma at the interdigital level of the left paw. The injection site was masked to avoid the stealing count phenomenon. Both the pathway and the ipsilateral pre-scapular lymph node are visible, this last is therefore considered the sentinel lymph node.

Fig. 39. - SPECT in a dog undergoing to thyroidal study.

dogs [178].

In conclusion, the use of Nuclear Medicine in Veterinary practice is still challenging. If it is true that these techniques are used in many Veterinary academic institutions, there are many difficulties with their application in clinical practice, mainly related to the high cost, the regulations and the operators specific training.

Declaration of Competing Interest

The authors declare that they have no known competing financial interests or personal relationships that could have appeared to influence the work reported in this paper.

Acknowledgment

The authors thank Prof. Antonella Volta of the University of Parma for MRI images and Prof. Davide Zani and Dr. Donatella de Zani of the University of Milan for Nuclear Imaging images within our manuscript.

References

[1] B. Marincek, S.W. Young, Computed tomography of spontaneous canine neoplasms, Vet. Radiol. 21 (4) (1980) 181–184.
[2] J. Fike, R. LeCouteur, C. Cann, Anatomy of the canine brain using high resolution computed tomography, Vet. Radiol. Ultrasound 22 (1981) 236–243.
[3] S. Ohlerth, G. Scharf, Computed tomography in small animals - basic principles and state of the art applications, Vet. J. 173 (2007) 254–271.
[4] T. Schwarz, Artifacts in CT (Veterinary Computed Tomography), in: T. Schwarz, J. Saunders (Eds.), Veterinary Computed Tomography, 1st ed., Wiley Blackwell, 2011, pp. 35–55 (Veterinary Computed Tomography).
[5] C. Lee, P.L. Guichet, F. Abtin, Percutaneous lung biopsy in the molecular profiling era a survey of current practices, J. Thorac. Imaging 32 (2017) 63–67.
[6] C. Le Roux, N. Cassel, G.T. Fosgate, A.L. Zwingenberger, R.M. Kirberger, Computed tomographic findings of pulmonary atelectasis in healthy anesthetized Beagles, Am. J. Vet. Res. 77 (10) (2016) 1082–1092.
[7] K.M. Lascola, S.C. Clark-Price, S.K. Joslyn, M.A. Mitchell, R.T. O'Brien, S. K. Hartman, K.H. Kline, Use of manual alveolar recruitment maneuvers to eliminate atelectasis artifacts identified during thoracic computed tomography of healthy neonatal foals, Am. J. Vet. Res. 77 (11) (2016) 1276–1287.
[8] J.C. Jones, S.E. Davies, S.R. Werre, K.L. Shackleford, Effects of body position and clinical signs on L7-S1 intervertebral foraminal area and lumbosacrale angle in dogs with lumbosacral disease as measured via computed tomography, Am. J. Vet. Res. 69 (2008) 1446–1454.
[9] C. Murino, G. Mennonna, L. Meomartino, Computed tomographic features in canine elbow dysplasia, Vet. Imag. Rev. 2 (1) (2016) 18–22.
[10] a) J.P. Farese, R.J. Todhunter, G. Lust, A.J. Williams, N.L. Dykes, Dorsolateral subluxation of hip joints in dogs measured in a weight-bearing position with radiography and computed tomography, Vet. Surg. 27 (5) (1998) 393–405; b) C.R. Oliveira, F.N. Ranallo, G.J. Pijanowski, et al., The VetMouseTrapTM: a device for computed tomographic imaging of the thorax of awake cats, Vet. Radiol. Ultrasound 52 (2011) 41–52.
[11] M. Gumpergerg, W. Henninger, The use of computed tomography in avian and reptile medicine, Semin. Avian Exot. Pet. Med. 10 (4) (2001) 174–180.
[12] S.M. Puchalski Adv. Equine Comput. Tomogr. Use Contrast Media, Vet. Clin.: Equine Pract. 28 3 2012 563 581.
[13] J. Saunders, T. Schwarz. Principles of CT Images Interpretation, in Veterinary Computed Tomography, 1st ed., Wiley Blackwell, 2011, pp. 29–34.
[14] R. Pollard, S. Puchalski. CT Contrast Media and Application, in Veterinary Computed Tomography, 1st ed., Wiley Blackwell, 2011, pp. 57–65.
[15] S. Scarabelli, P. Cripps, E. Rioja, B. Alderson, Adverse reactions following administration of contrast media for diagnostic imaging in anaesthetized dogs and cats: a retrospective study, Vet. Anaesth. Analg. 43 (5) (2016) 502–510.
[16] K.L. Basher, R. Porter, M. Martin-Flores, Severe (grade IV) hypersensitivity to iodinated contrast agent in an anesthetized dog, Can. Vet. J. 60 (7) (2019) 766–769.
[17] S.M. Stieger-Vanegas, L. Cladwell, J.A. Vanegas, E. McKenzie, J. Johns, Clinical Utility of abdominal multidetector CT in 85 goats with suspected abdominal disease, Vet. Radiol. Ultrasound 63 (4) (2022) 403–413.
[18] G. Piegari, E. D'Anza, D. Costanza, F. Prisco, L. Meomartino, I. d'Aquino, S. Albarella, O. Paciello, F. Ciotola, Perosomus elumbis in piglets: pathological, radiological and cytogenetic findings, Animals 11 (4) (2021) 1132.
[19] E. Epperly, J.A. Whitty, Equine imaging: computed tomography interpretation. Veterinary clinics of North America, Equine Pract. 36 (3) (2020) 527–543.
[20] K. Nuss, C. Schnetzler, R. Hagen, A. Schwarz, P. Kircher, Clinical application of computed tomography in cattle Tierarztl. Prax. Ausg. G: Gross – Nutztier 39 5 2011 317 324.

[21] B. de Vilbiss, D. Neelis, J. Ochoa, J. Ziegler, G. Barrington, A. Allen, Computed tomography findings in a 5-year-old Australian Cashmere goat (*Capra hircus*) suffering leukoencephalomyelitis due to caprine arthritis encephalitis virus. Canadian, Vet. J. 54 (2013) 960–964.

[22] R. Mao, H. Qi, L. Pei, J. Hao, J. Dong, T. Jiang, A. Ainiwaer, G. Shang, L. Xu, X. Shou, S. Zhang, G. Wu, P. Lu, Y. Bao, H. Li, CT scanning in identification of sheep cystic echinococcosis, BioMed. Res. Int. (2017), ID4639202.

[23] Ø. Nordbø, R. Sagevik, J. Kongsro, K. Mikkelsen, A.B. Gjuvsland, A. Gaustad, D. Olsen, E.W. Remme, E. Grindflek, A high-throughput study of visceral organs in CT-scanned pigs, Sci. Rep. 12 (2022) 9154.

[24] T. Banzato, T. Hellebuyck, A. Van Caelenberg, J.H. Saunders, A. Zotti, A review of diagnostic imaging of snakes and lizards, Vet. Rec. 173 (2013) 43–49.

[25] V. Capello, Diagnostic Imaging of Dental Disease in Pet Rabbits and Rodents, Vet. Clin. North Am. Exot. Anim. Pract. 19 (3) (2016) 757–782.

[26] G. Woods, N.I. Gunz, I. Handel, T. Liuti, R.J. Mellanby, T. Schwarz, Computed tomography osteodensitometry for assessment of bone mineral density of the canine head-preliminary results, Animals 11 (2021) 1413.

[27] L. Bünger, C. Glasbey, G. Simm, J. Conington, J. Macfarlane, K. McLean, K. Moore, N. Lambe, Use of X-ray Computed Tomography (CT) in UK Sheep Production and Breeding, INTECH Open Access Publisher, 2001.

[28] G. Pastorelli, S. Panseri, G. Curone, A. Zanon, M. Di Giancamillo, Imaging, sensory properties and fatty acid composition of Parma ham and "Nero di Parma" ham, Ital. J. Food Sci. 31 (2) (2019) 401–415.

[29] P. Moissonier, S. Blot, P. Devauchelle, et al., Stereotactic CT-guided brain biopsy in the dog, J. Small Anim. Pract. 43 (2002) 115–123.

[30] C.W. Dewey, Encephalopathies: disorders of the brain, in: C.W. Dewey (Ed.), A Practical Guide to Canine and Feline Neurology, Iowa State Press, 2003.

[31] L. Motta, M.T. Mandara, G.C. Skerritt, Canine and feline intracranial meningiomas: an updated review, Vet. J. (2012) 153–165.

[32] A.D. Miller, C.R. Miller, J.H. Rossmeisl, Canine primary intracranial cancer: a clinicopathologic and comparative review of glioma, meningioma, and choroid plexus tumors, Front. Oncol. 9 (2019) 1151.

[33] J.M. Snyder, F.S. Shofer, T.J. Van Winkle, C. Massicotte, Canine intracranial primary neoplasia: 173 cases (1986-2003), J. Vet. Intern. Med. 20 (3) (2006) 669–675.

[34] P.V. Scrivani. Veterinary Head and Neck Imaging, first ed., Wiley Blackwell, 2022.

[35] S. Ohlerth, B. Kaser-Hotz, Computed tomography as an aid in the management of tumors in small animals, Kleintierpraxis 46 (1) (2001) 5–14.

[36] B. Kaser-Hotz, C.R. Rohrer, S. Stankeova, M. Wergin, J. Fidel, C. Reusch, Radiotherapy of pituitary tumours in five cats, J. Small Anim. Pract. 43 (7) (2002) 303–307.

[37] C.M. Estey, Congenital hydrocephalus, Vet. Clin. Small Anim. 46 (2016) 217–229.

[38] S.A. Arnold, S.R. Platt, K.P. Gendron, F.D. West, Imaging ischemic and hemorrhagic disease of the brain in dogs, Front. Vet. Sci. 7 (2020) 279.

[39] E.M. de Lucas, E. Sánchez, A. Gutiérrez, A.G. Mandly, E. Ruiz, A.F. Flórez, J. Izquierdo, J. Arnáiz, T. Piedra, N. Valle, I. Bañales, F. Quintana, CT protocol for acute stroke: tips and tricks for general radiologists, Radiographics 28 (6) (2008) 1673–1687.

[40] M. Ahmed, T.J. Masaryk, Imaging of acute stroke: state of the art, Semin. Vasc. Surg. 17 (2) (2004) 181–205.

[41] V. Drago, G. Fatone, A. Testa, S. Reale, O. Paciello, L. Meomartino, CT assessment in canine meningoencephalomyelitis, Vet. Res. Commun. 32 (1) (2008) S279–S281.

[42] L.R. Talarico, S.J. Schatzberg, Idiopathic granulomatous and necrotising inflammatory disorders of the canine central nervous system: a review and future perspectives, J. Small Anim. Pract. 51 (3) (2010) 138–149.

[43] C. Malinowski, Canine and feline nasal neoplasia, Clin. Tech. Small Anim. Pract. 21 (2) (2006) 89–94.

[44] M. Fink, F. Ponce, L. Guilbaud, C. Chervier, F. Floch, J.L. Cadoré, T. Chuzel, M. Hugonnard, Computed Tomography or rhinoscopy as the first-line procedure for suspected nasal tumor: a pilot study, Can. Vet. J. 56 (2) (2015) 185–192.

[45] J. Lefebvre, N.F. Kuehn, A. Wortinger, Computed tomography as an aid in the diagnosis of chronic nasal diseasein dogs, J. Small Anim. Pract. 46 (6) (2005) 280–285.

[46] W.C. Schoenborn, E.R. Wisner, P.P. Kass, M. Dale, Retrospective assessment of computed tomographic imaging of feline sinonasal disease in 62 cats, Vet. Radiol. Ultrasound 44 (2) (2003) 185–195.

[47] J.N. Winer, F.J.M. Verstraete, D.D. Cissell, C. Le, N. Vapniarsky, K.L. Good, C. J. Gutierrez, B. Arzi, Clinical features and computed tomography findings are utilized to characterize retrobulbar disease in dogs, Front. Vet. Sci. 21 (5) (2018) 186.

[48] B.A. Jones, N. Cotterill, R. Drees, U.M. Dietrich, Purzycka: Tumours involving the retrobulbar space in cats: 37 cases, J. Feline Med. Surg. 24 (6) (2022) e116–e123.

[49] L. Barachetti, C.M. Mortellaro, M. Di Giancamillo, C. Giudice, P. Martino, O. Travetti, P.E. Miller, Bilateral orbital and nasal aspergillosis in a cat, Vet. Ophthalmol. 12 (3) (2009) 176–182.

[50] C. Giordano, P. Gianella, S. Bo, A. Vercelli, C. Giudice, D. Della Santa, A. M. Tortorano, C. Peruccio, A. Peano, Invasive mould infections of the naso-orbital region of cats: a case involving Aspergillus fumigatus and an aetiological review, J. Feline Med. Surg. 12 (9) (2010) 714–723.

[51] A. Belmudes, C. Pressanti, P.Y. Barthez, E. Castilla-Castaño, L. Fabries, M. C. Cadiergues, Computed tomographic findings in 205 dogs with clinical signs compatible with middle ear disease: a retrospective study, Vet. Dermatol. 29 (1) (2018) 45–e20.

[52] O. Travetti, C. Giudice, V. Greco, R. Lombardo, C.M. Mortellaro, Di, M. Giancamillo, Computed Tomography features of middle ear cholesteatoma in dogs, Vet. Radiol. Ultrasound 51 (4) (2010) 374–379.

[53] R.C. da Costa, V.F. Samii, Advanced imaging of the spine in small animals, Vet. Clin. North Am. Small Anim. Pract. 40 (5) (2010) 765–790.

[54] N.J.H. Sharp, M. Cofone, I.D. Robertson, A. DeCarlo, G.K. Smith, D.E. Thrall, Computed Tomography in the evaluation of caudal cervical spondylomyelopathy of the doberman pinscher, Vet. Radiol. Ultrasound 36 (2) (1995) 100–108.

[55] M. Ricciardi, A. Campanella, G. Grieco, R. Zammit, Usefulness of spinal unenhanced computed tomography and CT-myelography in the age of multidetector CT technology and magnetic resonance imaging - Preliminary considerations, Open Vet. J. 8 (3) (2018) 265–281.

[56] J.C. Jones, P.K. Shires, K.D. Inzana, D.P. Sponenberg, C. Massicotte, W. Renberg, A. Giroux, Evaluation of canine lumbosacral stenosis using intravenous contrast-enhanced computed tomography, Vet. Radiol. Ultrasound 40 (2) (1999) 108–114.

[57] C.M. Ruoff, S.C. Kerwin, A.R. Taylor, Diagnostic imaging of discospondylitis, Vet. Clin. North Am. Small Anim. Pract. 48 (1) (2018) 85–94.

[58] M. Hebel, W.K. Panek, J.J. Ruszkowski, M. Nabzdyk, D. Niedzielski, K.C. Pituch, A.M. Jackson, M. Kiełbowicz, M. Pomorska-Mól, Computed tomography findings in a cohort of 169 dogs with elbow dysplasia - a retrospective study, BMC Vet. Res. 17 (1) (2021) 296.

[59] J.K. Reichle, R.D. Park, A.M. Bahr, Computed Tomographic findings of dogs with cubital joint lameness, Vet. Radiol. Ultrasound 41 (2) (2000) 125–130.

[60] S.I. Wang, K.G. Mathews, I.D. Robertson, M. Stebbins, B.J. Trumpatori, The effects of patient positioning and slice selection on canine acetabular angle assessment with computed tomography, Vet. Radiol. Ultrasound 46 (1) (2005) 39–43.

[61] M.M.D. Ginja, A.J. Ferreira, S.S. Jesus, P. Melo-Pinto, J. Bulas-Cruz, M.A. Orden, F. San-Roman, M.P. Llorens-Pena, J.M. Gonzalo-Orden, Comparison of clinical, radiographic, computed tomographic, and magnetic resonance imaging methods for early prediction of canine hip laxity and dysplasia, Vet. Radiol. Ultrasound 50 (2) (2009) 135–143.

[62] I. Masseau, C.R. Reinero, Thoracic computed tomographic interpretation for clinicians to aid in the diagnosis of dogs and cats with respiratory disease, Vet. J. (253) (2019).

[63] Nomina Anatomica Veterinaria, Sixth edition – 2017. ⟨http://www.wava-amav.org/wava-documents.html⟩.

[64] J. Caswell, K. Williams, Respiratory system, in: G.M. Maxie (Ed.), Jubb, Kennedy and Palmer's Pathology of Domestic Animals, Elsevier Saunders, Philadelphia, PA, USA, 2007, p. 525.

[65] R.J. Rose, D.R. Worley, A contemporary retrospective study of survival in dogs with primary lung tumors: 40 cases (2005-2017), Front. Vet. Sci. Vol. 7 (2020).

[66] J.H. Harvey, Mammary glands, in: M.J. Bojrab, G.W. Ellison, B. Slocum (Eds.), Current Techniques in Small Animal Surgery, Williams & Wilkins, Baltimore, 1998, pp. 579–584.

[67] C.S. Hedlund, Mammary neoplasia. Small animal surgery T.W. Fossum St. Louis 2007 Elsevier Mosby 729 735.

[68] T. Schwarz, V. Johnson, "Lungs and Bronchi", in Veterinary Computed Tomography, in: T. Schwarz, J. Saunders (Eds.), Veterinary Computed Tomography, first ed., Wiley Blackwell, 2011, pp. 261–277.

[69] M. Cerquetella, F. Laus, E. Paggi, T. Zuccari, A. Spaterna, B. Tesei, Bronchial vegetal foreign bodies in the dog – localization in 47 cases, J. Vet. Med. Sci. 75 (7) (2013) 959–962.

[70] S.W. Atwater, B.E. Powers, R.D. Park, R.C. Straw, G.K. Ogilvie, S.J. Withrow, Thymoma in dogs: 23 cases (1980–1991), J. Am. Vet. Med. Assoc. 205 (1994) 1007–1013.

[71] G.S. Starrak, C.R. Berry, R.L. Page, J.L. Johnson, D.E. Thrall, Correlation between thoracic radiographic changes and remission/survival duration in 270 dogs with lymphosarcoma, Vet. Radiol. Ultrasound 38 (6) (2017) 411–418.

[72] J. Yoon, D.A. Feeney, D.E. Cronk, K.L. Anderson, L.E. Ziegler, Computed tomographic evaluation of canine and feline mediastinal masses in 14 patients, Vet. Radiol. Ultrasound 45 (6) (2004) 542–546.

[73] A.M. McGrath, S.A. Salyer, A. Seelmann, Ap Lundberg, M.R. Leonard, J. N. Lorbach, S. Lumbrezer-Johnson, E.T. Hostnik, G. Tremolada, J. Lapsley, L. E. Selmic, Mediastinal fibrosarcoma in a Dog – Case report, Front. Vet. Sci. Vol 9 (2022).

[74] M.J. Day, Review of thymic pathology in 30 cats and 36 dogs, J. Small Anim. Pract. 38 (1997) 393–403.

[75] G.W. Ellison, M.M. Garner, N. Ackerman, Idiopathic mediastinal cyst in a cat, Vet. Radiol. Ultrasound 35 (1994) 347–349.

[76] D.E. Thrall, The mediastinum, in: D.E. Thrall (Ed.), Textbook of Veterinary Diagnostic Radiology, W.B. Saunders Company, Philadelphia, 2018, pp. 649–669.

[77] T.C. Watton, A. Lara-Garcia, C.R. Lamb, Can malignant and inflammatory pleural effusions in dogs be distinguished using computed tomography? Vet. Radiol. Ultrasound 58 (5) (2017) 535–541.

[78] J.A. Reetz, E.L. Buza, E.L. Krick, CT features of pleural masses and nodules, Vet. Radiol. Ultrasound 53 (2) (2011) 121–127.

[79] Francis Barr Robert O'Brien "Abdominal Imaging" in BSAVA Manual of Canine and Feline Abdominal Imaging BSAVA Ed. 2009 1 4.

[80] K. Fukushima, H. Kanemoto, K. Ohno, M. Takahashi, K. Nakashima, Y. Fujino, K. Uchida, R. Fujiwara, R. Nishimura, H. Tsujimoto, CT characteristics of primary hepatic mass lesions in dogs, Vet. Radiol. Ultrasound 53 (3) (2015) 252–257.

[81] R. Leela-Arpon, H. Ohta, G. Shimbo, N. Sasaki, M. Takiguchi, Morphometric evaluation of canine hepatocellular carcinoma using computed tomography: a promising tool for predicting malignancy, J. Vet. Med. Sci. 83 (9) (2019) 1459–1464.

[82] T. Tanaka, H. Yamazaki, K. Ashida, Y. Limori, K. Mie, H. Nishida, H. Akiyoshi, Computed tomography may detect liver infiltration of canine diffuse hepatic lymphoma, Vet. Med. Sci. 7 (6) (2021) 2172–2177.
[83] A.C. Berent, K.M. Tobias, Portosystemic vascular anomalies, Vet. Clin. North Am. Small Anim. Pract. 39 (3) (2009) 513–541.
[84] A. Zwingenberger, CT diagnosis of portosystemic shunts, Vet. Clin. North Am. Small Anim. Pract. 39 (4) (2009) 783–792.
[85] S. Hoey, R. Drees, S. Hetzel, Evaluation of the gastrointestinal tract in dogs using computed tomography, Vet. Radiol. Ultrasound 54 (1) (2013) 25–30.
[86] M. Gualtieri, M.G. Monzeglio, E. Scanziani, Gastric neoplasia, Vet. Clin. North Am. Small Anim. Pract. 29 (2) (1999) 415–440.
[87] S.J. Withrow, Cancer of the gastrointestinal tract D.M. Vail Saunders Withrow and MacEwen's Small Animal Clinical Oncology 2012.
[88] E. Scanziani, A.M. Giusti, M. Gualtieri, D. Fonda, Gastric carcinoma in the Belgian shepherd dog, J. Small Anim. Pract. 32 (9) (1991) 465–469.
[89] H.M. Swann, D.E. Holt, Canine gastric adenocarcinoma and leiomyosarcoma: A retrospective study of 21 cases (1986-1999) and literature review, J. Am. Vet. Med. Assoc. 38 (2) (2002) 157–164.
[90] M.D. Willard, Alimentary neoplasia in geriatric dogs and cats, Vet. Clin. North Am. Small Anim. Pract. 42 (4) (2012) 693–706.
[91] T. Tanaka, H. Akiyoshi, K. Mie, M. Okamoto, Y. Yoshida, S. Kurokawa, Contrast-enhanced computed tomography may be helpful for characterizing and staging canine gastric tumors, Vet. Radiol. Ultrasound 60 (1) (2019) 7–18.
[92] M. Zuercher, F. Vilaplana Grosso, A. Lejeune, Comparison of the clinical, ultrasound, and CT findings in 13 dogs with gastric neoplasia, Vet. Radiol. Ultrasound 62 (5) (2021) 525–532.
[93] R. Terragni, M. Vignoli, F. Rossi, P. Laganga, V.F. Leone, J.P. Graham, M. Russo, J.H. Saunders, Stomach wall evaluation using helical hydro-computed tomography, Vet. Radiol. Ultrasound 53 (4) (2012) 402–405.
[94] B.M. Miniter, A.G. Arruda, J. Zuckerman, A.V. Caceres, R. Ben-Amotz, Use of computed tomography (CT) for the diagnosis of mechanical gastrointestinal obstruction in canines and felines, PLoS One 14 (8) (2019), e0219748.
[95] P.J. Watson, A.J.A. Roulois, T. Scase, P.E.J. Johnston, H. Thompson, M. E. Herrtage, Prevalence and breed distribution of chronic pancreatitis at post-mortem examination in first-opinion dogs, J. Small Anim. Pract. 48 (11) (2007) 609–618.
[96] A.M. Adrian, D.C. Twedt, S.L. Kraft, A.J. Marolf, Computed tomographic angiography under sedation in the diagnosis of suspected canine pancreatitis: a pilot study, J. Vet. Intern. Med. 29 (1) (2015) 97–103.
[97] J.M. French, D.C. Twedt, S. Rao, A. Marolf, Computed tomographic angiography and ultrasonography in the diagnosis and evaluation of acute pancreatitis in dogs, J. Vet. Intern. Med. 33 (2019) 79–88.
[98] L.L. Head, G.B. Daniel, T.J. Becker, D.A. Lidbetter, Use of computed tomography and radiolabeled leukocytes in a cat with pancreatitis, Vet. Radiol. Ultrasound 46 (3) (2005) 263–266.
[99] A.S. Tidwell, D.G. Penninck, J.G. Besso, Imaging of adrenal gland disorders, Vet. Clin. North Am. Small Anim. Pract. 27 (2) (1997) 237–254.
[100] D.S. Rosenstein, Diagnostic Imaging in canine pheocromocytoma, Vet. Radiol. Ultrasound 41 (6) (2000) 499–506.
[101] G. Bertolini, T. Furlanello, M. Drigo, M. Caldin, Computed Tomographic adrenal gland quantification in canine adrenocorticotroph hormone-dependent hyperadrenocorticism, Vet. Radiol. Ultrasound 49 (5) (2008) 449–453.
[102] T. Gregori, P. Mantis, L. Benigni, S.L. Priestnall, C.R. Lamb, Comparison of computed tomographic and pathologic findings in 17 dogs with primary adrenal neoplasia, Vet. Radiol. Ultrasound 56 (2) (2015) 153–159.
[103] W.D. Fife, V.F. Samii, W.T. Drost, J.S. Matoon, S. Hoshaw-Woodard, Comparison between malignant and non-malignant splenic masses in dogs using contrast-enhanced computed tomography, Vet. Radiol. Ultrasound 45 (4) (2004) 289–297.
[104] S. Burti, A. Zotti, F. Bonsembiante, B. Contiero, T. Banzato, A machine learning-based approach for classification of focal splenic lesions based on their CT features, Front. Vet. Sci. (2022).
[105] T. Tanaka, H. Akiyoshi, H. Nishida, K. Mie, L.S. Lin, Y. Limori, M. Okamoto, Contrast-enhanced computed tomography findings of canine primary renal tumors including renal cell carcinoma, lymphoma, and hemangiosarcoma, PLoS One 14 (11) (2019), e0225211.
[106] M. Longo, M.E. Andreis, C. Pettinato, G. Ravasio, V. Rabbogliatti, D. De Zani, M. Di Giancamillo, D.D. Zani, Use of the bolus tracking technique for the tomographic evaluation of the uretero-vesicular junction in dogs and assessment of dose records, BMC Vet. Res. 12 (2016) 64.
[107] T. Schwarz, N. Bommer, M. Parys, F. Thierry, J. Bouvard, J. Perez-Accino, J. Saunders, M. Longo, Four-dimensional CT excretory urography is an accurate technique for diagnosis of canine ureteral ectopia, Vet. Radiol. Ultrasound 62 (2) (2021) 190–198.
[108] M. Russo, G.C.W. England, G. Catone, G. Marino, Imaging of canine neoplastic reproductive disorders, Animals 11 (5) (2021) 1213.
[109] C. Rowan, L. Cuddy, J. Bryan, R. Shiel, S. Hoey, Imaging diagnosis - computed tomography findings in a case of metastatic ovarian adenocarcinoma in a dog, Vet. Radiol. Ultrasound 58 (6) (2017) E60–E63.
[110] M.C.M. Barozzi, C.F. Saba, K.P. Gendron, CT characteristics of uterine and vaginal mesenchymal tumours in dogs, J. Small Anim. Pract. 62 (4) (2021) 293–299.
[111] G. Mantziaras, Imaging of the male reproductive tract, Theriogenology 150 (2020) 490–497.
[112] K. Haverkamp, L.K. Harder, N.S.M. Kuhnt, M. Lüpke, I. Nolte, P. Wefstaedt, Validation of canine prostate volumetric measurements in computed tomography determined by the slice addition technique using the Amira program, BMC Vet. Res. 4 (1) (2019) 15–49.
[113] R. Dennis, Magnetic resonance imaging and its application to veterinary medicine, Vet. Int. 5 (1993) 3–10.
[114] S.L. Kraft, P.R. Gavin, L.R. Wendling, V.K. Reddy, Canine brain anatomy on magnetic resonance images, Vet. Radiol. Ultrasound 30 (1989) 147–158.
[115] R. Drees, L.J. Forrest, R. Chappell, Comparison of computed tomography and magnetic resonance imaging for the evaluation of canine intranasal neoplasia comparative study, J. Small Anim. Pract. 50 (2009) 334–340.
[116] M. Karkkainen, L.U. Punto, R.M. Tulamo, Magnetic resonance imaging of canine degenerative lumbar spine diseases, Vet. Radiol. Ultrasound 34 (1993) 399–404.
[117] N. Hayashi, Y. Watanabe, T. Masumoto, et al., Utilization of low-"eld MR scanners, Magn. Reson. Med. Sci. 3 (2004) 27–38.
[118] M. Konar, J. Lang, Pros and cons of low-field magnetic resonance imaging in veterinary practice, Vet. Radiol. Ultrasound 52 (2011) S5–S14.
[119] A. Korbecki, A. Zimny, P. Podgórski, M. Sąsiadek, J. Bladowska, Imaging of cerebrospinal fluid flow: fundamentals, techniques, and clinical applications of phase-contrast magnetic resonance imaging, Pol. J. Radiol. 84 (2019) e240–e250.
[120] S. Cerda-Gonzalez, N.J. Olby, R. Broadstone, R. Broadstone, S. McCullough, Characteristics of cerebrospinal fluid flow in in Cavalier King Charles spaniels analyzed using phase velocity cine magnetic resonance imaging, Vet. Radiol. Ultrasound 50 (2009) 467–476.
[121] C. Hyunju, K. Yejin, H. Saebyel, C. Hojung, Cerebrospinal fluid flow in normal beagle dogs analyzed using magnetic resonance imaging, J. Vet. Sci. 22 (1) (2021), e2.
[122] M.A. Foster, Magnetic Resonance in Medicine and Biology, Pergamon Press, Oxford, 1984, pp. l–27.
[123] S.L. Kraft, P.R. Gavin, L.R. Wendling, V.K. Reddy, Canine brain anatomy on magnetic resonance images, Vet. Radiol. 30 (1989) 147–158.
[124] L.C. Hudson, L. Cauzinille, J.N. Kornegay, M.B. Tompkins, Magnetic resonance imaging of the normal feline brain, Vet. Radiol. Ultrasound 36 (1995) 267–275.
[125] W.B. Thomas, S.J. Wheeler, R. Kramer, Magnetic resonance imaging of primary brain tumors in dogs, Vet. Radiol. Ultrasound 37 (1996) 20–27.
[126] G.B. Cherubini, S.R. Platt, T.J. Anderson, C. Rusbridge, V. Lorenzo, P. Mantis, R. Cappello, Characteristics of magnetic resonance images of granulomatous meningoencephalomyelitis in 11 dogs, Vet. Rec. 159 (2006) 110–115.
[127] R.G. Lobetti, J.P. Pearson, Magnetic resonance imaging in the diagnosis of focal granulomatous meningoencephalitis in two dogs, Vet. Radiol. Ultrasound 37 (1996) 424–427.
[128] Y. Sawashima, K. Sawashima, Y. Taura, A. Shimada, T. Umemura, Clinical and pathological findings of a Yorkshire terrier affected with necrotizing encephalitis, J. Vet. Med. Sci. 58 (1996) 659–661.
[129] J.L. Buback, K.S. Schulz, M.A. Walker, Magnetic resonance imaging of the brain for diagnosis of neurocysticercosis in a dog, JAVMA 208 (1996) 1846–1848.
[130] W.B. Thomas, Nonneoplastic disorders of the brain, Clin. Tech. Small Anim. Pract. 14 (1999) 125–147.
[131] N.N. Baheti, A. Cherian, P.R. Wattamwar, C. Kesavadas, B. Thomas, Ischemic hyperintensities on T1-weighted magnetic resonance imaging of patients with stroke: new insights from susceptibility weighted imaging, Neurol. India 58 (2010) 90–94.
[132] W.B. Thomas, D.C. Sorjonen, R.O. Scheuler, Magnetic resonance of brain infarction in seven dogs, Vet. Radiol. Ultrasound 37 (1996) 345–350.
[133] W.B. Thomas, S.J. Wheeler, R. Kramer, Magnetic resonance imaging of primary brain tumors in dogs, Vet. Radiol. Ultrasound 37 (1996) 20–27.
[134] L. Motta, M.T. Mandara, G.C. Skerritt, Canine and feline intracranial meningiomas: an updated review, Vet. J. 192 (2012) 153–165.
[135] M. So-Jeung, K. Ju-Won, K. Byeong-Teck, L. Chae-Young, P. Hee-Myung, Magnetic resonance imaging findings of hepatic encephalopathy in a dog with a portosystemic shunt, J. Vet. Med. Sci. 74 (2012) 361–366.
[136] S. Kraft, E. Randall, M. Wilhelm, S. Lana, Development of a whole body magnetic resonance imaging protocol in normal dogs and canine cancer patients, Vet. Radiol. Ultrasound 48 (2007) 212–220.
[137] M. Wilfried, Diagnostic MRI in dogs and Cats, CRC Press, Boca Raton, 2018.
[138] L.S. Garosi, R. Dennis, T. Schwarz, Review of diagnostic imaging of ear diseases in the dog and cat, Vet. Radiol. Ultrasound 44 (2003) 137–146.
[139] M.P. Moore, P.R. Gavin, S.L. Kraft, C.E. DeHaan, C.W. Leathers, R.V. Dorn, MR, CT and clinical features from four dogs with nasal tumors involving the rostral cerebrum, Vet. Radiol. 32 (1991) 19–25.
[140] H. Van Bree, H. Degryse, B. Van Ryssen, F. Ramon, M. Desmidt, Pathologic correlations with magnetic resonance images of osteochondrosis lesions in canine shoulders, JAVMA 202 (1993) 1099–1105.
[141] W.R. Widmer, K.A. Buckwalter, E.M. Braunstein, et al., Radiographic and reso nance imaging of the stifle joint in experimental osteoarthritis of dogs, Vet. Radiol. Ultrasound 35 (1994) 371–383.
[142] E. Barrett, F. Barr, M. Owen, K. Bradley, A Retrosp, Study MRI Find. 18 dogs stifle Inj. Anim. Pr. 50 2009 448 455.
[143] D.K. Baird, J.T. Hathcock, P.F. Rumph, S.A. Kincaid, D.M. Visco, Low-field magnetic resonance imaging of the canine stifle joint: Normal anatomy, Vet. Radiol. Ultrasound 39 (1998) 87–97.
[144] C.C. Nordberg, K.A. Johnson, Magnetic resonance imaging of normal canine carpal ligaments, Vet. Radiol. Ultrasound 40 (1999) 128–136.
[145] L. Brogniez, R. Perrin, F. Hontoir, M. Vandeweerd, Vet. Prat. Equina (2020) 3–8.
[146] R.L. Tucker, S.N. Sampson, Magnetic resonance imaging protocols for the horse, Clin. Tech. Equine Pract. 6 (2007) 2–15.
[147] G.B. Daniel, Veterinary nuclear medicine, Semin Nucl. Med. 44 (2014) 2,3.
[148] A.K. LeBlanc, G.B. Daniel, Advanced imaging or veterinary cancer patience, Vet. Clin. North Am. Small Anim. Pract. 37 (2007) 1059–1077.

[149] J.J. Hoskinson, R.L. Tucker, Diagnostic Imaging of Lameness in Small Animals, Vet. Clin. North Am. Small Anim. Pract. 31 (2001) 165–180.
[150] G.B. Daniel, D.A. Neelis, Thyroid scintigraphy in veterinary medicine, Semin Nucl. Med. 44 (2014) 24–34.
[151] L.G. Barber, Thyroid tumors in dogs and cats, Vet. Clin. North Am. Small Anim. Pract. 37 (2007) 755–773.
[152] L.E. Quiney, J.L. Ireland, S.J. Dyson, Evaluation of the Diagnostic Accuracy of Skeletal Scintigraphy in Lame and Poorly Performing Sports Horses, Vet. Radiol. Ultrasound 59 (2018) 477–489.
[153] D.J. Barberini, M. Aleman, F. Aristizabal, M. Spriet, K.C. Clark, N.J. Walker, L. D. Galuppo, R.M. Amorim, K.D. Woolard, D.L. Borjesson, Safety and tracking of intrathecal allogeneic mesenchymal stem cell transplantation in healthy and diseased horses, Stem Cell Res. Ther. 9 (2018) 96.
[154] F. Morandi, P.A. Sura, D. Sharp, G.B. Daniel, Characterization of multiple acquired portosystemic shunts using transplenic portal scintigraphy, Vet. Radiol. Ultrasound 51 (2010) 466–471.
[155] A.C. Berent, K.M. Tobias, Portosystemic vascular anomalies, Vet. Clin. North Am. Small Anim. Pract. 39 (2009) 513–541.
[156] G.B. Daniel, R. Bright, E. Monnet, P. Ollis, Comparison of per-rectal portal scintigraphy using 99m-technetium pertechnetate to mesenteric injection of radioactive microsheperes for quantification of portosystemic shunts in an experimental dog model, Vet. Radiol. 31 (1990) 175–181.
[157] P.D. Koblik, J. Komtebedde, C.K. Yen, W.J. Hornof, Use of transcolonic 99mtechnetium-pertechnetate as a screening test for portosystemic shunts in dogs, J. Am. Vet. Med. Assoc. 196 (1990) 925–930.
[158] P.D. Koblik, W.J. Hornof, C.K. Yen, J. Komtebedde, E. Breznock, P. Fisher, Comparison of shunt fraction estimation using transcolonic iodine-123-iodoamphetamine and technetium-99m-pertechnetate in a group of dogs with experimentally-induced chronic biliary cirrhosis, J. Nucl. Med. 32 (1991) 124–129.
[159] G.B. Daniel, A. Bahr, J.A. Dykes, R. De Novo, K. Young, G.T. Smith, Hepatic extraction efficiency and excretion rate of technetium-99m-mebrofenin in dogs, J. Nucl. Med. 37 (1996) 1846–1849.
[160] J.M. French, A. Brody, D. von Stade, C.B. Frank, L.R. Griffin, Flourine-18 fluorodeoxyglucose positron emission tomography imaging exhibits increased SUVmax at the level of the spinal intumescence in normal dogs, Vet. Radiol. Ultrasound 61 (2020) 364–369.
[161] J. Lawrence, E. Rohren, J. Provenzale, PET/CT today and tomorrow in veterinary cancer diagnosis and monitoring: fundamentals, early results and future, Perspect. Comp. Oncol. 8 (2010) 163–187.
[162] S.M. Seiler, C. Baumgartner, J. Hirschberger, A.J. Beer, A. Brühschwein, N. Kreutzmann, S. Laberke, M.C. Wergin, A. Meyer-Lindenberg, J. Brandl, A. K. von Thaden, E. Farrell, M. Schwaiger, Comparative oncology: evaluation of 2-deoxy-2-[18F]fluoro-D-glucose (FDG) positron emission tomography/computed tomography (PET/CT) for the staging of dogs with malignant tumors, PLoS One 10 (2015).
[163] A. Borgatti, A.L. Winter, K. Stuebner, R. Scott, C.P. Ober, K.L. Anderson, D. A. Feeney, D.A. Vallera, J.S. Koopmeiners, J.F. Modiano, J. Froelich, Evaluation of 18-F-fluoro-2-deoxyglucose (FDG) positron emission tomography/computed tomography (PET/CT) as a staging and monitoring tool for dogs with stage-2 splenic hemangiosarcoma - a pilot study, PLoS One 12 (2) (2017), e0172651. Feb 21.
[164] H. Voshikawa, E.K. Randall, S.L. Kraft, S.M. Larue, Comparison between 2-(18) F-fluoro-2-deoxy-d-glucose positron emission tomography and contrast-enhanced computed tomography for measuring gross tumor volume in cats with oral squamous cell carcinoma, Vet. Radiol. Ultrasound 54 (2013) 307–313.
[165] J.L. Willcox, M. Spriet, A.L. Zwingenberger, K.L. Phillips, J.H. Burton, K. A. Skorupski, K.S. Hansen, V.K. Affolter, K.D. Woolard, D. Beylin, M.A. Giuffrida, Evaluation of accuracy for (18) F-FDG positron emission tomography and computed tomography for detection of lymp hnode metastasis in canine oral malignant melanoma, Vet. Comp. Oncol. 19 (2021) 463–472.
[166] L.R. Griffin LR, D.H. Thamm, A. Brody, L.E. Selmic, Prognostic value of fluorine (18) flourodeoxyglucose positron emission tomography/computed tomography in dogs with appendicular, J. Vet. Intern. Med. 33 (2019) 820–826.
[167] M. Spriet, J.L. Willcox, W.T.N. Culp, Role of positron emission tomography in imaging of non-neurologic disorders of the head, neck, and teeth in veterinary medicine, Front. Vet. Sci. 6 (2019) 180.
[168] M. Manfredi, D. De Zani, L.E. Chiti, R. Ferrari, D. Stefanello, C. Giudice, V. Pettinato, M. Longo, M. Di Giancamillo, D.D. Zani, Preoperative planar lymphoscintigraphy allows for sentinel lymph node detection in 51 dogs improving staging accuracy: feasibility and pitfalls, Vet. Radiol. Ultrasound 62 (2021) 602–609.
[169] J.J. Hoskinson, R.L. Tucker, Diagnostic imaging of lameness in small animals, Vet. Clin. North Am. Small Anim. Pract. 31 (2001) 165–180.
[170] E. McLarty, M. Spriet, D. Beylin, P.Y. Chou, B. Filliquist, D.J. Marcellin-Little, A. S. Kapatkin, Comparison of 18F-sodium fluoride positron emission tomography and CT: an exploratory study in 12 dogs with Elbow pain, Vet. Radiol. Ultrasound 62 (2021) 498–506.
[171] M.S. Suh, S.H. Park, Y.-K. Kin, P.Y. Yun, W.W. Lee, ^{18}F-NaF PET/CT for the evaluation of temporomandibular joint disorder, Clin. Radiol. 73 (2018) 1–7.
[172] M. Spriet, P. Espinosa, A.Z. Kyme, K.L. Phillips, S.A. Katzman, L.D. Galuppo, et al., ^{18}F-sodium fluoride positron emission tomography of the equine distal limb: exploratory study in three horses, Equine Vet. J. 50 (2018) 125–132.
[173] M. Norvall, P. Spriet, G. Espinosa, B.G. Ariño-Estrada, S.A. Murphy, L.D. Katzman Galuppo, Chondrosesamoidean ligament enthesopathy: prevalence and findings in a population of lame horses imaged with positron emission tomography, Equine Vet. J. 53 (2021) 451–459.
[174] P. Spriet, D.D. Espinosa-Mur, K.L. Cissell, G. Phillips, D. Arino-Estrada, P. Beylin, S.A. Stepanov, L.D. Katzman, T. Galuppo, B. Garcia-Nolen, S.M. Murphy Stover, ^{18}F-sodium sluoride positron emission tomography of the racing thoroughbred fetlock: validation and comparison with other imaging modalities in nine horses, Equine Vet. J. 51 (2019) 375–383.
[175] S. Wilson, M. Spriet, P.E. Mur, S. Anishchenko, D. Beylin, S. Katzman, L. Galuppo, ^{18}Fluorine-fluorodeoxyglucose Positron Emission Tomography for assessment of deep digital flexor Tendinopathy: An exploratory study in Eight Horses with comparison to CT and MRI, Vet. Radiol. Ultrasound 62 (2021) 610–620.
[176] A.K. LeBlanc, K. Peremans, PET and SPECT imaging in veterinary medicine, Semin. Nucl. Med. 44 (2014) 47–56.
[177] M.F. van den Berg, S. Daminet, E. Stock, E. Vandermeulen, S. Scheemaeker, M. Campos, H.S. Kooistra, S. Galac, L. Duchateau, K. Peremans, Planar and single-photon emission computed tomography imaging in dogs with thyroid tumors: 68 cases, J. Vet. Intern. Med. 34 (2020) 2651–2659.
[178] S. Vermeire, K. Audenaert, E. Vandermeulen, T. Waelbers, B. De Spiegeleer, H. van Bree, K. Peremans, Single photon emission computed tomography (SPECT) imaging of the dopamine transporter in healthy dogs, Vet. J. 188 (2011) 356–358.